



Micro- and nano-environments of carbon sequestration: Multi-element STXM-NEXAFS spectromicroscopy assessment of microbial carbon and mineral associations

Dawit Solomon ^{a,*}, Johannes Lehmann ^a, Jennifer Harden ^b, Jian Wang ^c, James Kinyangi ^a, Karen Heymann ^a, Chithra Karunakaran ^c, Yingshen Lu ^c, Sue Wirick ^d, Chris Jacobsen ^e

^a Cornell University, Ithaca, NY, 14853, USA

^b United States Geological Survey, Menlo Park, CA 94025, USA

^c Canadian Light Source Inc, Saskatoon, SK, Canada S7N 0X4

^d National Synchrotron Light Source, Brookhaven National Laboratory, Upton, NY 11973, USA

^e Advanced Photon Source, Argonne National Laboratory, Argonne, IL 60439, USA

ARTICLE INFO

Article history:

Accepted 2 February 2012

Available online 10 February 2012

Keywords:

Biotic exclusion zone

Long-term C sequestration

Global C cycling

Organomineral interactions

X-ray spectromicroscopy

ABSTRACT

Soil represents the largest reservoir of terrestrial organic C, and plays a critical role in global C cycling. In light of predicted climate change and a more unified approach to mitigate greenhouse gas emissions, the soil's ability to sequester C, and thus to act as a sink or a source for atmospheric CO₂ has received growing interest. Organomineral assemblages are a unique niche in C cycling, with large capacity for storing anthropogenic C. However, the underlying biogeochemical mechanisms for C sequestration through organomineral associations are not yet well understood. One of the major challenges to study C sequestration in organomineral assemblages is lack of non-invasive analytical tools with a potential to obtain molecular-level information about the interactions between C and mineral components in submicron geochemical environments. In the present study, we have effectively employed synchrotron-based STXM-NEXAFS spectroscopy to access the K- and L-edges of biogeochemically relevant elements (C, N, Ca, Fe, Al, Si) to identify and image micro- and nano-C sequestration environments, and conduct submicron-level investigation of the compositional chemistry and other interactive features of C and minerals present in these hotspots using ultrathin section of intact organomineral assemblage. The C K-edge NEXAFS spectromicroscopy micrographs clearly demonstrated the existence of spatially distinct seemingly terminal micro- and nano-C repository zones, where organic C was sequestered in apparent agglomeration in the investigated organomineral assemblage. These submicron-C repository environments were only a few micrometers apart from each other; yet they were considerably different compositionally from each other. The organic C in the first repository environment was pyrogenic in origin, largely composed of quinone, phenols, ketones and aromatic ring structures. However, the second hotspot was dominated by filament-like structure, with striking similarity to the C 1s NEXAFS spectral signatures of organic C isolated from soil fungal and bacteria, and dominated by resonances from aliphatic-C and C=N bonds of imidazol structures, carboxyl/carbonyl-C, amide- and O-alkyl-C functionalities. The composition of organic C in the organomineral interface around the strand-like structure was highly complex and composed of polysaccharides, amino sugars, amino acids, nucleic acids, and phospholipid fatty acid structures with polar and non-polar termini. The chemistry of mineral matter in the organomineral interface was also equally complex, ranging from Ca, Fe and Al ions, Fe and Al oxides, hydroxides and oxyhydroxides to phyllosilicates, which could provide a variety of polyvalent cations, hydroxyl surface functional groups and edge sites that can attract and bind microbial biomolecules. Based on the enormous complexity of the organic C functionalities and the coexistence of various inorganic components in the organomineral interface, it is possible to suggest that no single binding mechanism could be accountable for the organic C stored in the investigated submicron-C repository environment. Our results seem to suggest that the apparent C sequestration in the micro- and nano-C repository environment appear to be the cumulative result of physical protection and heterogeneous binding mechanisms ranging from ion exchange, hydrogen bonding, and hydrophobic bonding on silicate clay-organic complexes to adsorption on external and internal surfaces of clay minerals.

© 2012 Elsevier B.V. All rights reserved.

* Corresponding author at: Cornell University, Ithaca, NY 14853, USA. Tel.: +1 607 255 1730; fax: +1 607 255 2644.

E-mail address: ds278@cornell.edu (D. Solomon).

1. Introduction

Soil represents the largest reservoir of terrestrial organic C on the global scale, and plays a critical role in global C cycling. It contains 4.3 times the size of the atmospheric pool (760 Gt), 5.9 times the size of the biotic pool (560 Gt); and current estimates of the global soil organic C pool are in the order of 3300 Gt in the top 3 m (Tarnocai et al., 2009). Organic C enters the soil system as a heterogeneous mixture of organic molecules composed of compounds released from living plant and microbial cells to complex plant, animal and microbial residues ranging in size and complexity from simple monomers to complex biopolymers (Solomon et al., 2007a). Most of this C is readily mineralized by microorganisms within a short timescales of one or two years (Jenkinson and Ladd, 1981). The remaining portion, however, can be stabilized for longer timescales of up to thousands of years (Sollins et al., 1996). In light of predicted climate change and a more unified approach to mitigate greenhouse gas emissions, the soil's ability to retain C, and thus to act as a sink or a source for increasing anthropogenic CO₂ concentrations in the atmosphere has received growing interest in the last decades (Lal, 2004). Despite its importance, however, the underlying biogeochemical mechanisms for the long-term stabilization of C in soils are not yet well understood; and the full potential for C sequestration in the Earth's surface remains unknown (Trumbore, 2009).

The dominant mechanisms affecting the stability of organic C in soils are typically categorized into three major processes: (i) selective preservation of primary and secondary refractory C compounds (ii) spatial inaccessibility of organic C to microbes and enzymes due to localized occlusions by microaggregation, intercalation within phyllosilicates, and encapsulation in pore spaces, and (iii) inter-molecular associations between organic C and minerals or metal ions. Selective preservation due to recalcitrance leads to a progressive change of detritus composition during the initial stage of decomposition. However, it does not explain the long-term stabilization of potentially labile organic C substrates in soils; and it is increasingly seen as a transient process (Sollins et al., 1996; Baldock and Nelson, 2000). Literature evidence increasingly seems to suggest that organic C stabilization caused by organomineral associations and “biotic exclusion” due to substrate inaccessibility to decomposing organisms, many of which occur only at micro- and nano-environments, appears to be the dominant process (Horn and Smucker, 2005). Smucker et al. (2007) indicated that some of these “biotic exclusion” zones are interconnected by a range of intra-aggregate nano-sized pores and could receive supplies of organic C from micro- and meso-pores in aggregates; yet prohibit on-site mineralization of C by bacteria and their associated enzymes. However, others are terminal and appear throughout microaggregates as “dead end” environments that may serve as C reservoirs in organomineral assemblages.

One of the major challenges to studying C sequestration in micro- and nano-environments is the lack of appropriate non-invasive analytical tools. Most of the information involving interfacial chemical processes and organomineral associations are inferred from bulk chemistry data generated by experimental approaches involving batch experiments, gas-sorption analysis or oxidative treatments (Templeton and Knowles, 2009). This information is used to build conceptual surface complexation and spatial allocation models to facilitate better understanding of C stabilization. While models built on evidence collected from destructive analytical approaches reveal important information, they usually fall short of providing explicit information about the linkage between mineralogy and organic C functionalities, as well as surficial and spatial allocations and other architectural features of organomineral assemblages (Sparks, 1995). Wan et al. (2007) indicated that without such direct submicron-level information, the mechanistic foundation for soil organic C stabilization as a result of organomineral associations remain largely lacking. Significant progress has been made in the past using

spectroscopy techniques such as X-ray photoelectron spectroscopy (XPS), Auger electron spectroscopy (AES) and secondary ion mass spectroscopy (SIMS). These approaches yield detailed information about the structure and bonding of minerals and the chemical species present on mineral surfaces (Amelung et al., 2002). However, many of these techniques are invasive, since experiments may need to be performed under adverse conditions (e.g., desiccation, heating, and particle bombardment) that may not simulate natural conditions in the soil environment; and could alter the nature of samples, yielding possibly misleading data as a result of experimental artifacts (Kögel-Knabner, 2000).

Scanning transmission X-ray microscopy (STXM), a powerful method created through advances in X-ray microfocusing and access to high-flux yet softer (~100 to 2000 eV) X-ray photons generated by a synchrotron light source, coupled with near-edge X-ray absorption fine structure (NEXAFS) spectroscopy provides an excellent opportunity to identify and fingerprint the fine structures of C and directly image micrometer sized environmental samples with nanometer spatial resolution (Jacobsen et al., 2000). More recently, STXM and NEXAFS spectromicroscopic analyses has been effectively employed to investigate soil C and mineral associations at a nanometer scale (Kinyangi et al., 2006; Lehmann et al., 2008). However, these studies were conducted at beamline optimized mostly for C, but lacking sufficient flux at higher energies to image Ca, Fe, Al and Si; which are among the most ubiquitous elements at the earth's surface and by far the most abundant mineral cations in soils, restricting the information generated from these investigations only to soil organic C. STXM–NEXAFS spectromicroscopy has potential to access the K- or L-edge of other elements (Ca, N, O, Fe, Al, Si etc.); and may lead to acquisition of multi-element and spatially defined high resolution (<50 nm; Wan et al., 2007; Thieme et al., 2010) mechanistic information for geobiological investigations involving C and minerals or polyvalent metal ions associations, as well as other surficial and interactive features occurring in organomineral assemblages (Solomon et al., 2009).

Therefore, the objectives of this investigation were: (i) to identify and image the locations of micro- and nano-environments of organic C sequestration in ultrathin section of intact organomineral assemblage of a mineral soil, (ii) to fingerprint the fine structures of C present in these complex C repository environments, and (iii) to conduct a submicron-level investigation of the compositional chemistry and interactions of the various elements (N, Ca, Fe, Al and Si) present in the organomineral interface with organic C that may have relevance for long-term stabilization of soil C using a non-destructive high resolution STXM and NEXAFS spectromicroscopy.

2. Materials and methods

2.1. Study site description and sample background information

The present study was conducted using soil samples collected from the Kakamega forest ecosystem of western Kenya. Kakamega forest is located at 00°14'19"N and 34°57'13"E and represents the eastern-most remnant of Guineo-Congolian rainforest. The altitude of the area ranges from 1700 to 1800 m above sea level, with mean annual temperature of 19 °C and precipitation of 2080 mm. The natural vegetation is composed of tropical (e.g., *Aningeria altissima* (A. Chev.), *Milicia excelsa* (Welw., C.C. Berg), and *Chrysophyllum albidum* (G. Don)), and montane (e.g., *Olea capensis* (L.) and *Croton megalocarpus* (Hutchinson)) forest species. The soils of the area developed from undifferentiated basement system rocks. They are well-drained, deep red to yellowish red, friable sandy clay loam to clay loam texture with 400 g kg⁻¹ sand, 210 g kg⁻¹ silt and 380 g kg⁻¹ clay; and classified as Ferralo-Chromic Acrisols (FAO-UNESCO, 1997). The organic C content was 119 g kg⁻¹ soil, total N was 11 g kg⁻¹ soil, total S was 2.9 g kg⁻¹ soil, with pH-KCl of 5.3 and bulk density of 0.79 g cm⁻³.

Krull et al. (2002) indicated that these soils are dominated by Fe Al and Si; with relatively lower Ca, K, and Mg contents. Detailed chemical and mineralogical properties can be found in Krull et al. (2002) and Solomon et al. (2007a, 2009).

2.2. Ultrathin section preparation

One gram of undisturbed soil was sieved to pass through a 250 µm sieve but trapped on a 150 µm sieve, and the free stable microaggregates in this range were isolated. The microaggregates were then sprinkled on a glass fiber filter (Whatman GF/A, 90 mm diameter), mounted onto a 1000 µm sieve surface; and fixed to a chimney funnel that transferred mist from a humidifier (Ultra-violet light, Slant/Fin; 7.5 L capacity). The humidifier chamber was filled with double deionized Millipore water dispensed from a Barnstead NanoPure Diamond water purification system (Thermo Fisher Scientific, Waltham, Massachusetts, USA) to hydrate the microaggregates. After 18 h of continuous misting, the microaggregates were considered to be water saturated. Excess droplets on the glass fiber filter were drained off before shock-freezing the microaggregates. This procedure enabled the spatial arrangement of organic matter in soils to be observed at high resolution without compromising the spatial integrity of the organomineral assemblage (Lehmann et al., 2008). An approximately 150 µm diameter microaggregate subsample was selected and submitted to the cryomicrotome for ultrathin sectioning. Since the pretreatment results in a frozen sample, sectioning was accomplished at -55°C . Sectioning to a thickness of 400 nm was done with an ultramicrotome (Ultracut UTC, Leica Microsystems Inc, Bannockburn, Illinois, USA) using a glass knife for initial trimming and a diamond knife (MS9859 Ultra 45 °C, Diatome Ltd., Biel, Switzerland) for final cutting at 1.2 mm s^{-1} (cutting angle of 6°). The ultrathin sections were transferred using an eyelash probe (Christensen, 1971) to a silicon monoxide (SiO) impregnated copper (Cu) transmission electron microscopy grid (200 meshes, No. 53002, Ladd Research, Williston, Vermont, USA). The Cu grid was mounted onto the center pinhole of stainless steel sample stage plates (46 mm diameter) for STXM measurements. Details about the thin sectioning procedure are described by Kinyangi et al. (2006).

2.3. Multi-element STXM and NEXAFS data acquisition and analysis

2.3.1. C K-edge spectromicroscopy

The C K-edge NEXAFS spectromicroscopy measurements were recorded at X1A1 beamline of the National Synchrotron Light Source (NSLS), Brookhaven National Laboratory (BNL) using the STXM end station. The essential components of this beamline are a tunable undulator inserted in the 2.8 GeV electron storage ring generating a high flux of photons at 10^7 spatially coherent photons s^{-1} in the soft X-ray region, a spherical grating monochromator with maximum spectra resolving power of 5000 lines mm^{-1} , a 160-µm Fresnel zone plate that can focus the beam to a 40 nm spot size for a maximum spatial resolution of up to 50 nm, and a proportional counter to detect the transmitted photons. The beamline slit width was set to 45/25/25 µm to provide an energy resolution of 0.1 eV. Both spectral and imaging resolutions of the beamline are described in depth elsewhere (Wirick et al., 2009). The monochromator was calibrated using CO_2 adsorption band (290.7 eV). A stack data set was collected in transmission mode under He atmosphere by imaging in X and Y dimensions, then changing the monochromator by energy increments of 0.3 eV for the energy range from 280.0 to 282.5 eV (dwell time, DT, 1 ms), 0.1 eV from 282.6 to 292.0 eV (DT, 2 ms), 0.5 eV from 292.1 to 305.5 eV (DT, 3 ms) and 1.0 eV from 305.6 to 310.0 eV (DT, 4 ms). Smaller energy step (0.1 eV) was chosen at levels where core electrons of C can be excited (283.0–290.0 eV). The dwell time was increased to improve counting statistics at spectroscopically interesting regions, in regions where samples showed high absorbance, or in

regions where the incident flux is low. After the entire microaggregate was scanned using a zone plate with 40 nm focused beam spot at 500 nm steps (for clarity from here on described as 500 nm spatial resolution), high-resolution scans were conducted at the various C repository zones or hotspots within the intact micro-organomineral assemblage at a 50 nm spatial resolution (40 nm focused beam spot and at 50 nm steps) to probe these micro- and nano-C sequestration environments (Kinyangi et al., 2006; Lehmann et al., 2008; Wirick et al., 2009). Individual images recorded across all energy levels were built into a stack using the Stack Analyze 2.6.1 software (Jacobsen et al., 2000), then aligned in X and Y using cross-correlation (with 290.0 eV as a reference). For the spatial analyses, the stack data were orthogonalized and noise-filtered by principal component analysis as described in Lerotic et al. (2004) and Kinyangi et al. (2006). Cluster analysis was used to identify sample regions with similar spectral properties and to identify regions for which target spectra of total organic C were defined in comparison with cluster spectra using PCA GUI 1.1.1 program (Lerotic et al., 2004). The first 4 components and 12 clusters were used on the basis of the eigenvalues, eigenimages and eigenspectra (Lerotic et al., 2004; Kinyangi et al., 2006; Lehmann et al., 2008) calculated by the principal component analysis, without using the first principal component as described in Kinyangi et al. (2006). Cluster analysis uses this subset of principal components to group similar spectra in the stack data set (Lerotic et al., 2004), and produce cluster maps. Singular value decomposition (SVD) was performed to calculate target maps and corresponding fitted target spectra from the spectra obtained by cluster analysis. Stack image processing software and data analyses instructional manuals can be accessed on the web at <http://xray1.physics.sunysb.edu/data/software.php>.

2.3.2. N, Al, Si K-edge, and Ca and Fe L-edge spectromicroscopy

The N, Al, Si K-edge, and Ca and Fe L-edge NEXAFS spectromicroscopy measurements were performed using STXM end station at the soft X-ray spectromicroscopy (SM) 10ID-1 beamline of the Canadian Light Source (CLS) located at the University of Saskatchewan. The 10ID-1 beamline, inserted in 2.9 GeV electron storage ring, consists of an APPLE II type Elliptically Polarizing Undulator (EPU), a Plane Grating Monochromator (PGM) optimized for photons from 100 to 2000 eV range. The STXM provides high quality imaging and spatially resolved spectroscopy with an on-sample flux of 10^8 photon s^{-1} focused by a Fresnel zone plate lens to a 30 nm focal spot sizes, with a 30 nm spatial resolution and spectral resolution power ($E/\Delta E$) that can reach up to $\sim 10,000$. Details about the STXM principle and design of the microscope can be found at Kaznatcheev et al. (2007), Karunakaran (2009) and at http://www.lightsource.ca/experimental/pdf/SM_Beamline_Technical_Sheet.pdf. Stack data set for Ca L-edge, N K-edge, Fe L-edge, Al K-edge and Si K-edge NEXAFS spectromicroscopy were collected in transmission mode under He atmosphere from the ultrathin section used for C K-edge NEXAFS. Similar to C, image sequences were recorded in X and Y dimensions and then changing the monochromator in energy increments varying from 0.3 to 0.88 eV (depending on the element analyzed) first from the entire microaggregate using a zone plate with a focused spatial resolution of 500 nm, and latter high-resolution (50 nm) scans were recorded at the same micro- and nano-regions identified using the center X and Y coordinates and ranges of the C NEXAFS images. The increasing energy flux and stack energy range parameters for the high-resolution scans performed at CLS are provided as follows: (i) Ca L-edge 340.0–343.5 eV at 0.3 eV steps, 343.6–354.0 eV at 0.1 eV and 354.1–360.0 eV at 0.3 eV steps with 27/27 µm slit size and 1 ms DT, (ii) N K-edge 390.0–395.0 eV at 1 eV steps, 395.1–404.0 eV at 0.1 eV steps, 404.1–410.0 eV at 0.3 eV, and 411.1–430.0 at 1 eV steps with 27/27 µm slit size and 0.87 ms DT, (iii) Fe L-edge 700.0–704.0 eV at 0.5 eV steps, 704.1–713.0 at 0.2 eV steps, 713.1–718.0 at 1 eV steps, and 718.1–735.0 eV steps at 1.5 eV

steps with 27/27 μm slit size and 0.87 ms DT, (iv) Al K-edge 1540.0–1558.0 eV at 1 eV steps, 1558.1–1575.0 at 0.2 eV steps, 1575.1–1585.0 at 1 eV steps, and 1585.1 1610.0 eV at 2 steps with 35/35 μm slit size and 0.87 ms DT, and (v) Si K-edge 1820.0–1830.0 eV at 1 eV steps, 1830.1–1860.4 at 0.2 eV steps, 1860.5–1880.5 at 0.5 eV steps, and 1880.6–1890.0 eV at 2 eV steps with 45/45 μm slit size and 0.95 ms DT. The high resolution stack data set was read and preprocessed using the stack fit and stack analyze routine of the Analysis of X-ray Microscopy Images and Spectra (aXis2000); an Interactive Data Language (IDL) widget for processing X-ray microscopy images and spectra developed by Hitchcock (2008). Additional image processing and data analyses instructions can be accessed at <http://unicorn.mcmaster.ca/aXis2000.html> to a format compatible with Stack Analyze (Jacobsen/Stony Brook V2.6.1, Jacobsen et al., 2000) and PCA GUI 1.1.1 (Lerotic et al., 2004) programs used for analyses C K-edge NEXAFS data. The image sequences were aligned and converted to optical density (OD) and principal component and cluster analysis for individual elements were conducted as described in Section 2.3.1 of this paper; and target and cluster maps, as well as spectra were produced for each element. The spectra were baseline corrected and normalized using WinXAS version 3.1 (WinXAS Soft ware, Hamburg, Germany) as described in Solomon et al. (2009).

3. Results and discussion

3.1. C K-edge STXM–NEXAFS spectromicroscopy

The spatially resolved C K-edge STXM–NEXAFS spectromicroscopy micrographs of the entire micro-organomineral assemblage (Fig. 1a) and the selected micro- and nano-C repository environments (Fig. 1b) showed a contrasting image of the distribution of total organic C (light gray) and mineral matter (dark gray) present within the investigated ultrathin section of an intact organomineral assemblage of a mineral soil. Although organic C was distributed throughout the entire micro-organomineral assemblage (Fig. 1a), closer inspection of the fine-scale distribution of C clearly showed a number of spatially distinct and seemingly terminal micro- and nano-repository zones or hotspots, where organic C was present in apparent agglomeration (Fig. 1bi and bii).

Differential analysis of the nano-scale spatial heterogeneity of C present in the selected submicron-level C reservoirs (Fig. 1bi and bii) revealed that the compositional chemistry of organic C present in these submicron-C repository zones was highly complex. According to Fig. 1, the composition of C present in the region with the filament-like morphology (Fig. 1bi), the details of which are the focus of this paper, appeared to be relatively low in energy bands associated with quinones (284.0–284.6 eV; Fig. 1c), characteristic transitions of aromatic ring structures (284.7–285.9 eV, Fig. 1d) and resonances related to phenols and ketones (286.0–286.9 eV, Fig. 1e). However, this region seems to be dominated by resonances related to aliphatic-C and imidazol ring structures (287.0–287.9 eV, Fig. 1f), carboxylic/carbonyl-C and amide functionalities (288.0–288.9 eV, Fig. 1g) and absorption bands related to O-alkyl-C (289.0–289.9 eV,

Fig. 1h) (Solomon et al., 1991; Brandes et al., 2004; Braun et al., 2007; Solomon et al., 2009). In contrast, the fine structure chemistry of C in the hotspot dominated by the more intact particulate organic structure (Fig. 1bii, the details of which is a subject of another article) was largely composed of quinone (Fig. 1c), aromatic ring structures (Fig. 1d) and resonances related to phenols and ketones (Fig. 1e). However, while transitions representing polysaccharides (Fig. 1h), carboxylic/carbonyl-C and amide functional groups (Fig. 1g), as well as aliphatic-C (Fig. 1f) were visible especially on the outer surface of this structure; they were largely less abundant compared to their presence in the hotspot dominated by the filament-like structure. These results indicate that the structural composition and morphology of organic C sequestered in micro- and nano-C repository zones of organomineral assemblages, which are far apart only by a few micrometers from each other, could be considerably different.

3.1.1. Cluster analysis of organic C from the filament-like structure

The spatially resolved C K-edge STXM–NEXAFS spectromicroscopy target map of the micro- and nano-organic C repository environment (Fig. 2a) clearly showed the filament-like organic structure (dark red) and the nearby organomineral interface (light gray) regions present within the investigated micro-organomineral assemblage. In addition, the cluster indices map (Fig. 2b) displayed various micro- and nano-regions with distinctively discernible C K-edge NEXAFS spectral features related to the exterior and interior regions of the filament-like structure (Fig. 2c–h) and the complex organomineral interface (Fig. 2i–m). The C K-edge spectra collected from the inner (Fig. 2c–d), intermediate (Fig. 2e–f) and outer (Fig. 2g–h) regions of the filament-like structure exhibited multiple peaks near 285.1 eV, 287.5 eV, 288.3 eV and 289.7 eV; with shoulders near 286.6 eV (Fig. 2n). The C 1s NEXAFS spectral signatures and peak positions recorded from the filament-like structure were strikingly similar to the spectral features observed from fungal hyphae and bacteria colonies isolated from soils by Liang et al. (2006) and Wirick et al. (2009). These results lead us to conclude that this micro- and nano-C repository environment could be dominated by organic C possibly originating from the strand-like structures of soil microorganisms and their metabolites. Our results are in line with the suggestion of Oades (1984), who pointed out that polysaccharide mucilage can be produced in situ by fungal hyphae and bacterial cells in the soil environment and exist in soil micro-environments as a gel or fibrillae; and may not diffuse or move around far from the site of production. Oades (1984) indicated that the mobile component in the interaction between mucilage and soil clay appears to be fine clay platelets; and the polysaccharides will either be encapsulated by the clay platelets or end up acting as glue binding the clay platelets to the strand-like microbial structure. The presence of microbial strand-like structures in intimate association with clay particles in organomineral assemblages have been also reported by Chenu and Stotzky (2002).

Detailed analysis of the spectral signatures of the filament-like structures revealed that resonances near 285.1 eV could be attributed to the π^* orbital of C ($\text{C } 1\text{s}-\pi^*\text{C}=\text{C}$) atoms originating from unsaturated C ($\text{C}=\text{C}$) bonds on aromatic ring structures (Table 1). These transitions might indicate the existence of aromatic protein

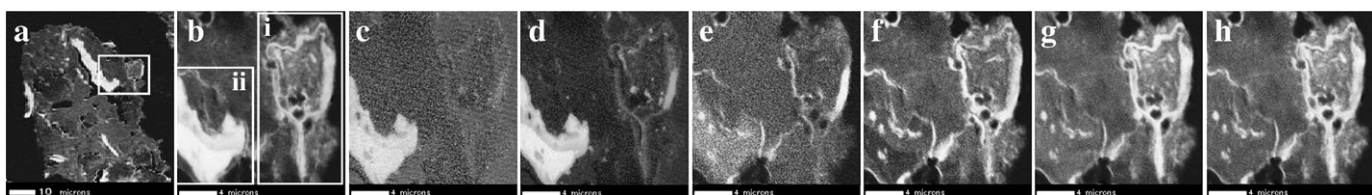


Fig. 1. C K-edge STXM–NEXAFS images of the entire intact organomineral assemblage (panel a) and the micro- and nano-C repository environments (panel b) showing spatial distribution of total C and mineral matter, and the fine-scale distribution of the various C functionalities (panel c, quinones; panel d, aromatic-C; panel e, phenols and ketones; panel f, aliphatic-C and imidazol structures; panel g, carboxylic/carbonyl and amide structures; panel h, polysaccharides and amino sugars) observed in the investigated organomineral assemblage.

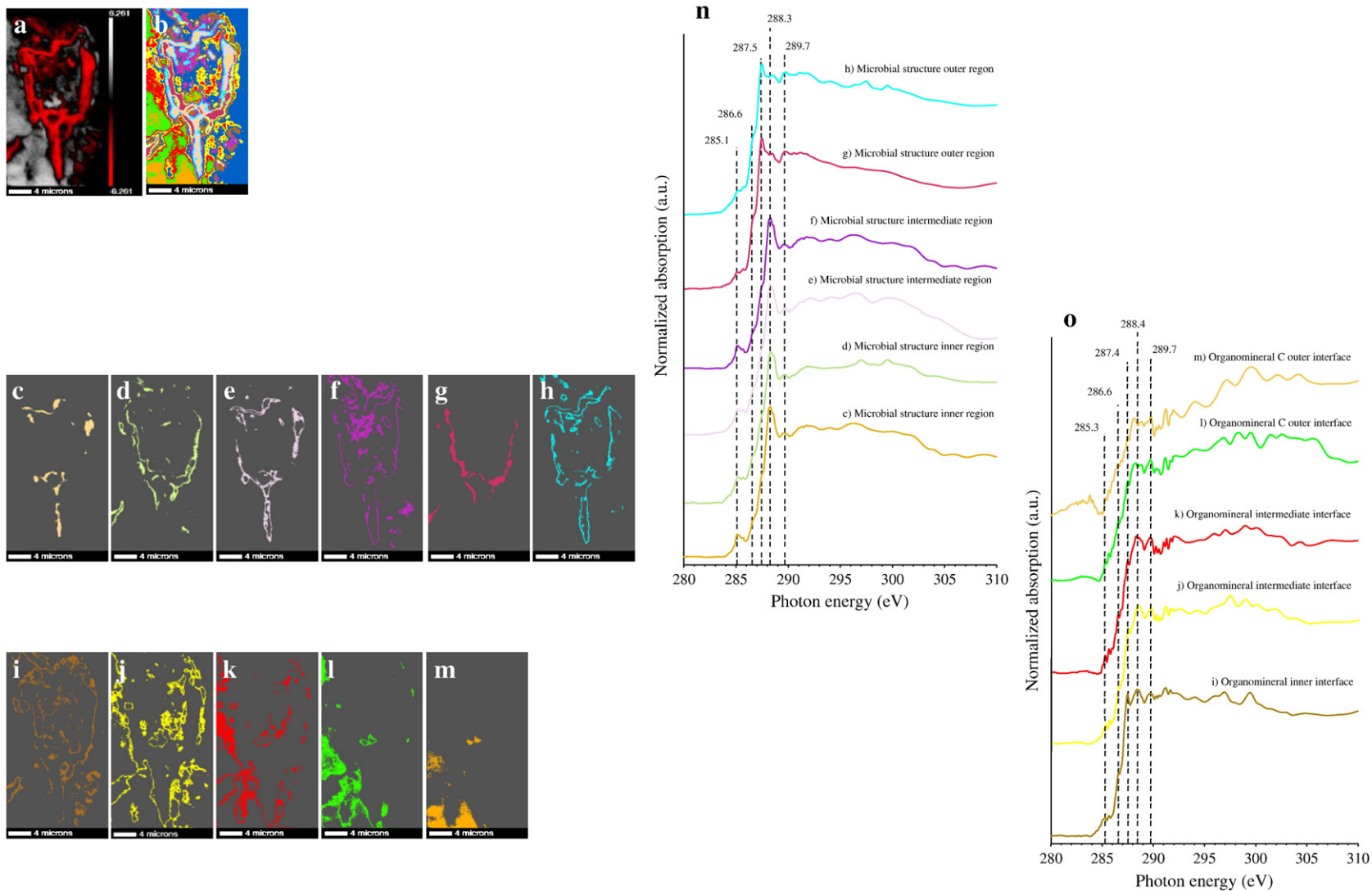


Fig. 2. High resolution C K-edge STXM-NEXAFS target (panel a) and cluster indices maps (panel b) of the investigated micro- and nano-C repository environment, individual cluster images of the various regions of the filament-like structure (panels c-h) and the nearby organomineral interface (panels i-m), and their respective C NEXAFS spectra (panels n and o).

Table 1

Photon energy ranges, transitions, the most likely functionalities and organic C forms identified by STXM–NEXAFS spectromicroscopy from the filament-like structure and nearby organomineral interface of the investigated organomineral assemblage.

Energy ranges eV	Functionalities	Transitions	Structures
<i>Filament-like structure</i>			
285.1–285.7	Aromatic-C Phenolic-C Ketonic-C Pyrrolic-C Aliphatic-C Amide-C Carboxylic/carbonyl-C Amide carbonyl-C	C 1s–π* _{C=C} C 1s–π* _{C=C} C 1s–π* _{C=O} C 1s–σ* _{C–N} C 1s–σ*/3p _{C–H} C 1s–π* _{C=N} C 1s–π* _{C=O} C 1s–π* _{C=O}	Aromatic ring structures of amino acids, proteins and nucleobases Aromatic-C connected to O group in phenols Carbonyl structures of ketones Pyrrole side ring structures of amino acids and nucleobase Aliphatic C functionalities of amino acids and phospholipid fatty acids Imidazol ring present in amino acids Carboxylic/carbonyl C of amino acids, amino sugars, polysaccharides Amide functionalities of nucleobases
286.5–286.7	O-alkyl-C Amide-C	C 1s–σ*/3p _{C–OH} C 1s–π* _{C=N}	O-alkyl-C moieties of amino sugars and polysaccharides Amide structures of amino acids
287.4–287.5			
288.0–288.7			
289.6–289.8			
<i>Organomineral interface</i>			
285.3–285.7	Aromatic-C Phenolic-C Ketonic-C Pyrrolic-C Aliphatic-C Amide-C Carboxylic/carbonyl-C Carboxyamide-C	C 1s–π* _{C=C} C 1s–π* _{C=C} C 1s–π* _{C=O} C 1s–π* _{C=N} C 1s–σ*/3p _{C–H} C 1s–π* _{C=N} C 1s–π* _{C=O} C 1s–π* _{C=O}	Aromatic ring structures of amino acids, proteins and nucleobases Aromatic-C connected to O atom of hydroxyl group in phenols Carbonyl structures of ketones Pyrrole side ring structures of amino acids CH, CH ₂ and CH ₃ groups of aliphatic C functionalities of amino acids Imidazol ring present in amino acids Carboxyl C in polysaccharides, phospholipid fatty acids and extracellular enzymes Amide functionalities and carboxyamide structures of nucleobases
286.5–286.6	O-alkyl-C Amide-C	C 1s–σ*/3p _{C–OH} C 1s–π* _{C=N}	O-alkyl-C of polysaccharides, protein-nucleic acid, alcohols and ethers Amide structures of amino acids, amino acids with alcohols and basic side chains
287.4–287.5			
288.1–288.9			
289.7–289.8			

macromolecules, amino acids with aromatic side chains such as phenylalanine, as well as from microbial nucleobases such as thymine that are building blocks of both deoxyribonucleic acid (DNA) and ribonucleic acid (RNA) (Francis and Hitchcock, 1992; Boese et al., 1997; Stöhr et al., 2001; Ade and Urquhart, 2002; Kaznacheyev et al., 2002; Solomon et al., 2007b; Solomon et al., 2009). The weakly developed shoulders near 286.6 eV (Table 1) could be attributed to the presence of C 1s–π*_{C=C} transitions of aromatic-C connected to the O atom (C-OH) of hydroxyl group as in the case of phenols, and to C 1s–π*_{C=O} transitions from carbonyl substituted aromatic structures of phenols and ketones (Braun et al., 2005; Samuel et al., 2006). These absorption bands could also arise due to C 1s–π*_{C=C} and C 1s–σ*_{C–N} transitions originating from pyrrole side ring structures of microbial amino acids such as tryptophan, nucleobases such as thymine, and to C 1s–π*_{C=N} transition of the C=N_x species of adenine (Kaznacheyev et al., 2002; Samuel et al., 2006; Solomon et al., 2009). The low energy shoulders that emerged near 287.5 of the filament-like structure could be ascribed to C 1s–σ*/3p_{C–H} Rydberg-like excitations from CH, CH₂ and CH₃ groups of aliphatic-C functionalities or they could also arise from π* resonances of C=N bonds from the imidazol ring present in amino acids such as histidine (Boese et al., 1997; Solomon et al., 2009). These structures appear to be much more prominent in the outer regions of the filament-like structure (Fig. 2n). Solomon et al. (2005) and Kinyangi et al. (2006) suggested that the presence of strong resonances from aliphatic-C chain structures together with oxidized carboxylic-and carbonyl-C structure could also be an indication for the occurrence of microbial C forms such as phospholipid fatty acids. The strong absorption bands near 288.3 eV in the inner and intermediate regions of the filament-like structure were assigned to C 1s–π*_{C=O} transitions of carboxyl/carbonyl-C (COOH/COO⁻) originating possibly from polysaccharides, amino sugars and amino acids, as well as amide (O=C–NH) functional groups common in nucleobases (Boyce et al., 2002; Kaznacheyev et al., 2002; Solomon et al., 2009). The resonances from these transitions appear to be very weak in the outer regions of the filament-like structures. The absorption bands near 289.6 eV correspond to the 1s–3p/σ* transitions of O-alkyl-C (C–OH) moieties primarily representing polysaccharides and amino sugars (Hitchcock and Mancini, 1994; Boyce et al., 2002). Solomon et al. (2009) demonstrated that the sharp absorption features between 289.1–289.6 eV

arise from transitions of C–OH molecular orbitals related to microbial polysaccharides such as deoxysugars, structural polymers of fungal cell-wall such as chitin, as well as N-acetyl muramic acid, which when interlinked by peptides can form peptidoglycan, a major constituent of bacterial cell walls. However, Kaznacheyev et al. (2002) reported that the C 1s–π*_{C=N} transitions of amino acids with side chains containing basic groups such as arginine could also result in a high energy peak around 289.2 eV, where the C=N C is bonded to three N atoms leading to a shift in the π* peak above that of a C 1s (COO⁻) site. The C K-edge spectra extracted from the cluster indices map of the filament-like structure did not exhibit spectral signatures related to the 1s–π*_{C=O} energy resonance associated with quinones commonly observed in pure compounds such as *p*-benzoquinone (Francis and Hitchcock, 1992; Solomon et al., 2009) or in complex environmental samples such as humic fractions or pyrogenic C present in soils (Braun et al., 2005; Solomon et al., 2005). Quinones are important organic compounds in the environment, which for the most part are produced through enzymatic oxidation of phenolic compounds such as lignin by polyphenoloxidases. Their absence, at least in this case, was further indication that microorganisms and their metabolites and not plant materials were the possible sources of organic C in this filament-like micro- and nano-C repository environment. These results are in line with the results of our differential analysis of the micro- and nano-scale spatial distribution of C in the filament-like structure.

3.1.2. Cluster analysis of C from the organomineral interface

The C K-edge spectra (Fig. 2o) collected from the inner, intermediate and outer regions of the organomineral interface (Fig. 2i–m) exhibited multiple pronounced resonances near 285.3 eV, 287.4 eV, 288.4 eV and 289.7 eV, and weakly developed shoulders near 286.6 eV. The absorption bands near 285.3 eV were assigned to the C 1s–π*_{C=C} transition of aromatic ring structure of microbial C associated most probably with amino acids, proteins and nucleobases; and often present in soils bound to mineral surfaces (Table 1; Wershaw and Pinckney, 1980; Kleber et al., 2007). The shoulders near 286.6 eV could be attributed to the presence of C 1s–π*_{C=C} transitions of phenols, and to C 1s–π*_{C=O} transitions from phenols and ketones present in the organomineral interface (Braun et al., 2005; Samuel et al., 2006). These absorption bands could also arise due to C

$1s-\pi^*_{C=C}$ and $C\ 1s-\sigma^*_{C-N}$ transitions of pyrrole side ring structures of microbial amino acids and nucleobase, and from the $C\ 1s-\pi^*_{C=N}$ transition of nucleobase present in the various regions of the organomineral interface near the filament-like organic structure (Kaznacheyev et al., 2002; Samuel et al., 2006; Solomon et al., 2009). The pronounced peaks near 287.3 eV, especially in the inner organomineral interface, could be indications for the presence of $C\ 1s-\sigma^*/3p_{C-H}$ Rydberg-like excitations of aliphatic-C species and π^* resonances of imidazol ring structures of amino acids and proteins. Kinyangi et al. (2006) observed the presence of $C\ 1s-\sigma^*/3p_{C-H}$ Rydberg-like transitions due to CH , CH_2 , and CH_3 groups of aliphatic-C in interior regions of organomineral coatings of microaggregates. These authors indicated that such components may form non-polar termini that confer hydrophobic properties and may lead to hydrophobic interaction between organic C and clay minerals leading to the adsorption of these compounds to the mineral layers in the organomineral complex. The broad resonances manifested near 288.4 eV could be attributed to the $C\ 1s-\pi^*_{C=O}$ from carboxyl-C ($COOH/COO^-$) and amide ($-CONH_2$) functional groups, and could signify the presence of C from polysaccharides, phospholipid fatty acids, extracellular enzymes and nucleobases present intimate association with the mineral matter (Benzerara et al., 2004; Solomon et al., 2005, 2009). Lawrence et al. (2003) and Benzerara et al. (2004) reported that the $C=O$ bond from the characteristic carboxyl phenyl ring of carboxyamides could also appear near 288.4 eV. The broader peaks near 288.4 eV from the intermediate and outer organomineral interface regions could be an indication for the presence of carboxyamides and signify the presence of both amide and polysaccharide carboxyl-C in the organomineral interface. In addition, Kaznacheyev et al. (2002) indicated that amino acids with side chains containing carboxylic and amine groups (e.g., cysteine and methionine) are characterized by $COOH$ π^* absorption band near 288.4 eV. Such amino acids predominantly form a zwitterionic structure, with a protonated amino (H_3N^+) and deprotonated carboxyl (COO^-) groups. Brash and Horbett (1995) and Kleber et al. (2007) indicated that numerous electrostatic bonds can form between reactive mineral sites and organic amide and other polar or charged functional groups during the adsorption process. Kinyangi et al. (2006) demonstrated that organic matter enriched with such protonated-deprotonated carboxyl termini ($COOH/COO^-$) could interact with mineral surfaces and form a discontinuous surface coat or thin film-like layer possibly through adsorption processes involving hydrogen bonding, van der Waals forces or electrostatic interactions (Chenu and Stotzky, 2002). The involvement of proteinaceous organic molecules stemming possibly from zwitterionic character of amino acids in certain forms of organomineral interactions and associations have been proposed by several researchers. Wershaw and Pinckney (1980) postulated that organic C is often bound to clay surfaces by amino acids or proteins. Similarly, Kleber et al. (2007) highlighted the formation of strong organomineral associations favored by situations, where either a polar organic functional group of amphiphilic interacts via ligand exchange with singly coordinated soil mineral surfaces or through processes involving proteinaceous materials unfolding upon adsorption to mineral surfaces, thus increasing adhesive strength by adding hydrophobic interactions to electrostatic binding. The C K-edge absorption bands that appeared near 289.7 eV corresponds to the $1s-3p/\sigma^*_{C-OH}$ transitions of O-alkyl-C ($CHOH$, CH_2-OH , CH_2-O-) structures (Table 1) possibly representing microbe related polysaccharides, protein-nucleic acid, as well as alcohols and ether bonded aliphatic-C structures present in the investigated organomineral interface regions. The occurrence of $C-OH$ molecular orbital related with relatively labile microbial polysaccharides, amino groups and other structural polymers of fungal and bacterial constituents in intimate association with the mineral interface in the investigate micro- and nano-C repository environment could be, therefore, direct evidence that such structures can be stabilized by organomineral complexes in mineral

soils. Chenu and Stotzky (2002) reported that microorganisms release extracellular polysaccharides and a number of other biologically active biomolecules such as extracellular enzymes, toxins and (deoxy)ribonucleic acids that have specific roles and targets in the soil environment. These microbial-derived exudates are susceptible to rapid and irreversible adsorption by soil particles, especially by clay minerals, mainly through weak bonds such as van der Waals forces and hydrogen bonding (Chenu, 1995). Electrostatic interactions are also involved in the case of charged extracellular polysaccharides, and di- or trivalent cations could enhance the adsorption of polysaccharides to charged clay minerals in the organomineral complex. The absorption bands near 289.8 eV could also arise from $C\ 1s-\pi^*_{C=N}$ due to the presence of amino acids with alcohol ($-OH$, e.g. threonine, serine) and mercapto ($-SH$, e.g. cysteine) or strongly basic ($(H_xN)_2-C=NH_2$; e.g. arginine) side chains (Kaznacheyev et al., 2002; Zubavichus et al., 2005). Kaznacheyev et al. (2002) stated that amino acids with alcohol side chain contain polar hydroxyl groups that can participate in hydrogen bond formation. Thus, such polar hydroxyl groups could also serve as a point of attachment in organomineral interactions and associations observed in the investigated micro- and nano-C repository environment. Overall, given the extraordinary diversity of organic C functionalities of the microbial organic matter present in the various regions of the organomineral interface, it is possible to suggest that the adsorption of microbial-C into the mineral matter and subsequent its sequestration in the investigated micro- and nano-C repository environment could be the cumulative result of heterogeneous binding mechanisms.

3.2. N K-edge STXM–NEXAFS spectromicroscopy

The spatially resolved high resolution N K-edge target map (Fig. 3b) of the investigated organomineral assemblage clearly showed the discernable features of the filament-like structure (light gray) and the nearby organomineral interface (dark red) regions, supporting the results from C K-edge STXM–NEXAFS spectromicroscopy. The N K-edge cluster indices map (Fig. 3c) revealed the micro- and nano-scale spatial distribution of the various N components with similar spectral properties at the inner, intermediate and outer regions of the filament-like structure (Fig. 3m), and the organomineral interface (Fig. 3n). Vairavamurthy and Wang (2002) and Samuel et al. (2006) reported that the N K-edge spectral features due to the transitions to the π^* orbitals occur at lower energies and they are characterized by sharp peaks compared to those arising due to transitions to σ^* orbitals. Thus, it is possible to suggest that the prominent absorption bands observed in the energy range of 399.1–404.0 eV from N K-edge spectra of the investigated micro- and nano-C repository environment could be assigned as representatives of the N $1s-\pi^*$ transitions, while the broader features observed at a higher energies (>405.0 eV) reflect the N $1s-\sigma^*$ resonances (Fig. 3m and n). These features were consistent throughout the experimental N K-edge spectra, indicating the presence of numerous N compounds in the submicron-C repository environment dominated by the filament-like structure and the nearby organomineral interface present within the investigated micro-organomineral assemblage.

3.2.1. Cluster analysis of N from the filament-like structure

The N K-edge spectra collected from inner (Fig. 3d), intermediate (Fig. 3e–f) and outer (Fig. 3g) regions of the filament-like microbial structure exhibited multiple peaks near 399.1 eV, 400.0 eV, 401.4 eV, 402.2 eV, 405.6 eV and 407.8 eV energy positions (Fig. 3m). The resonances near 399.1 eV could be attributed to the N $1s-\pi^*$ transitions from a variety of amino acids with aliphatic (e.g., alanine), alcohol (e.g., serine), mercapto (e.g., methionine), carboxylic (e.g., glutamic acids), aromatic (e.g., histidine) and strongly basic (e.g., arginine) side chains (Zubavichus et al., 2005). Leinweber et al. (2007) reported that amino sugars (e.g., N-acetyl-D-glucosamine

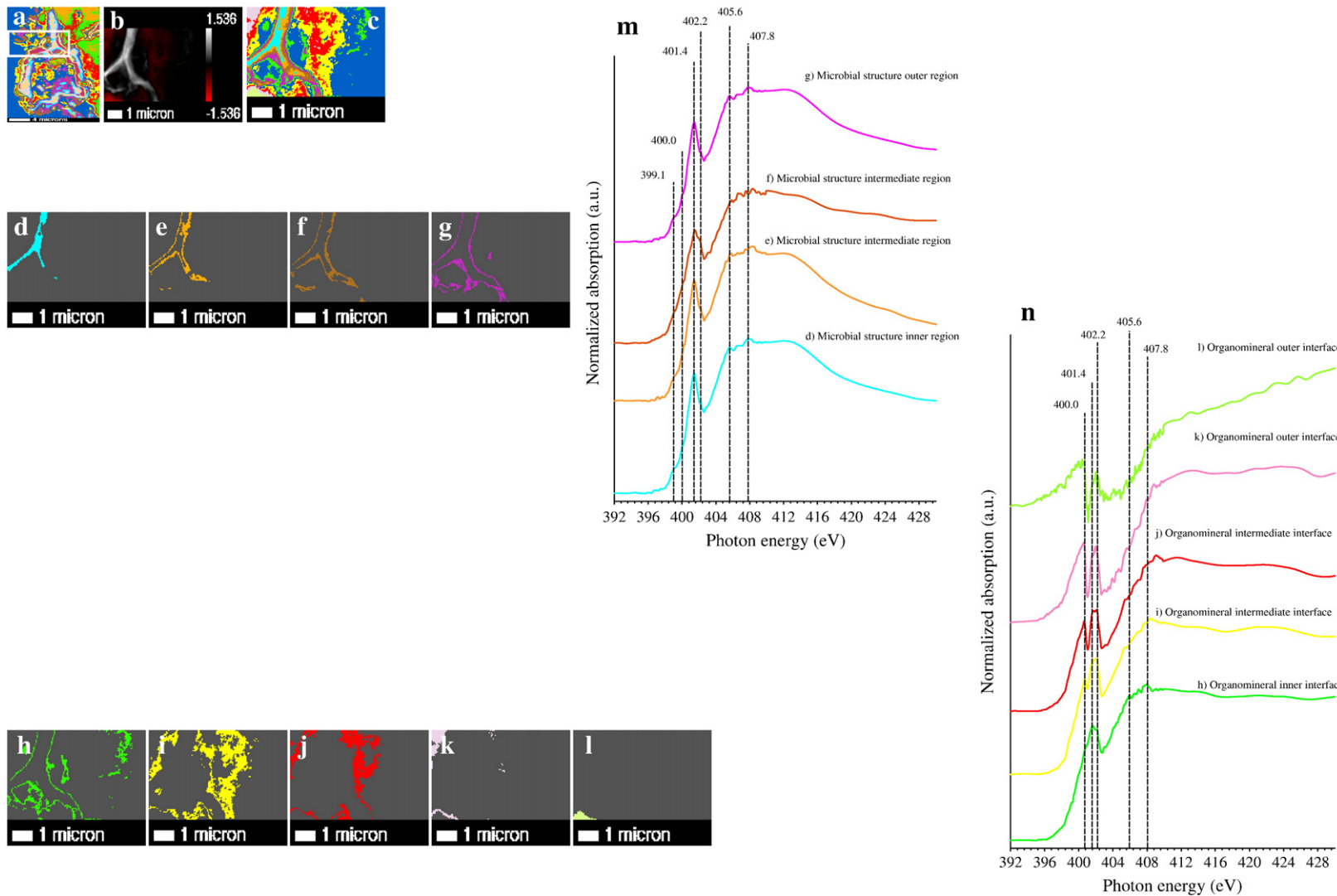


Fig. 3. High resolution C K-edge cluster indices map showing the region where N analysis was conducted (panel a), N K-edge NEXAFS target (panel b) and cluster indices (panel c) maps and individual N NEXAFS cluster images of the various regions of the filament-like structure (panels d–g) and the nearby organomineral interface (panels h–i), and their respective spectra (panels m and n).

and chitin), which are major constituents of fungal cell walls, as well heterocyclic N compounds associated with pyrimidine (e.g., thymine) and purine (e.g., adenine) structures could also show N 1s- π^* resonances in similar (i.e., 399.0–399.9 eV) energy range. The N 1s- π^* transitions near 400.0 eV could be attributed to heterocyclic N compounds with imidazole (e.g., L- β -imidazoleacetic acid) and pyrimidine (e.g., pyrazinecarboxamide, cytosine) structures derived from microbial metabolites. Amino acids with both basic and aromatic side chains were also shown to exhibit resonances around 400.0 eV (Leinweber et al., 2007). The N 1s- π^* absorption bands near 401.4 eV and 402.2 eV could be due to the presence of a variety of amino acids, amines and amides from N-acetyl-D-glucosamine and its polymer chitin to muramic acid, as well as from π^* resonances of heterocyclic N compounds associated with pyrimidine and purine structures related to microbial nucleic materials (Zubavichus et al., 2005; Samuel et al., 2006; Leinweber et al., 2007). The broad spectral features near 405.6 eV and 407.8 eV were possibly due to the N 1s- σ^* transitions of amino acids with aliphatic, alcohol, mercapto, carboxylic, aromatic and strongly basic side chains. These results seem to be in agreement with the results of Zubavichus et al. (2005) and Leinweber et al. (2007), who demonstrated that the spectra of the majority of amino acids are dominated by a relatively broad N 1s- σ^*_{N-C} peak extending from 405.0 eV to 409.0 eV. These authors indicated that in the cases of such amino acids as proline and hydroxyproline, this broad peak feature could apparently split into two components near 405.6 eV and 409.7 eV due to saturated N heterocycles. These spectral signatures could also be an indication for the presence of amines and amide functionalities originating possibly from amino sugars, which provide structural and functional roles for soil microorganisms, as well as from the π^* resonances of heterocyclic N compounds associated with pyrimidine and purine structures of microbial nucleobases (Solomon et al., 2001; Samuel et al., 2006). These results are clearly inline with our interpretation of the C K-edge spectral signatures of the filament-like structure, and support our previous suggestion that this strand-like structure and the organic C sequestered in the investigated micro- and nano-C repository environment originated possibly from the soil microorganisms and microbial metabolites.

3.2.2. Cluster analysis of N from the organomineral interface

The N K-edge spectra (Fig. 2n) collected from the inner, intermediate and outer regions of the organomineral interface present around the strand-like structure revealed multiple peaks near 400.0 eV, 401.4 eV, 402.2 eV, 405.6 eV and 407.8 eV energy positions. The N 1s- π^* transitions near 400.0 eV could indicate the presence of amino acids with basic and aromatic side chains in association with the mineral matter. These results could be further indication that the protonated and deprotonated termini of these proteinaceous organic compounds could interact with the mineral matter, and lead to the accumulation of these biomolecules in organomineral complex of the investigated micro- and nano-repository environment. The π^* resonance near 400.8 eV could also be contributions from heterocyclic microbial N compounds with imidazole and pyrimidine, as well as nitrile (R-C≡N) structures (Leinweber et al., 2007; Cody et al., 2008; Nuevoa et al., 2011) present in association with mineral component of the soil. The possible presence of long-chain alkyl nitriles, derived from long-chain fatty acids in soils have been also reported by Schulten and Schnitzer (1998) and Leinweber and Schulten (1998).

The N 1s- π^* spectral features near 401.4 eV and 402.2 eV, as well as from the broad N 1s- σ^* transitions near 405.6 eV and 407.8 eV clearly suggest that the organic material found in intimate association with the mineral matter was highly complex in its compositional chemistry. These N 1s- π^* spectral signatures indicate that this organic matter encompasses compounds ranging from amino acids with highly basic, aliphatic, alcohol carboxylic and aromatic side chains to amines and amide functionalities of amino sugar origin and

heterocyclic N species associated with pyrimidine and purine structures of RNA and DNA (Zubavichus et al., 2005; Samuel et al., 2006). The presence of amino acids, along with other organic constituents ranging from N-containing polysaccharides to protein-nucleic acids in the organomineral interface is in line with the findings of our C K-edge NEXAFS spectromicroscopy. It also provide further indication that these seemingly labile organic constituents could be released into submicron soil environments inaccessible to decomposing organisms as microbial exudates or as a product of biological membrane lysis; and could be sequestered in this seemingly terminal micro- and nano-C repository environments through simple bioexclusion. Huang (2004) stated that depending on the inherent properties of these microbial C species, they can also interact with the surfaces of the soil mineral interface through a variety of individual ion exchange mechanisms and accrue in the organomineral complex. Examples of such associations are the interactions between protonated amines and metallic cations occupying exchange sites on the surfaces of mineral colloids, and sorption of these moieties on mineral surfaces. Besides cation-exchange reactions, adsorption of organic constituents by mineral colloids may proceed through ionic, covalent, hydrophobic, hydrogen bonding, or even through van der Waals forces; although individual van der Waals forces are regarded as weak interactions. However, the retention mechanism could be also an action cumulative of all of these mechanisms, if these organic moieties are in close contact with the adsorbing surface composed of a wide variety of dissolved cations, oxides and hydroxides, as well as silicate clay components (Theng, 1979; Violante et al., 2002; Huang, 2004). Leinweber et al. (2007) and Gillespie et al. (2008) indicated that the 1s- π^* resonances near 401.6 eV and the broad N 1s- σ^* transitions near 405.8 eV could also originate from mineral N compounds such as ammonium phosphate ((NH₄)₃PO₄), nitrate (NH₄NO₃), sulfates ((NH₄)₂SO₄), as well as potassium (KNO₃) and calcium (Ca(NO₃)₂) nitrates. Thus, there is a possibility that the spectral signatures of such inorganic N compounds could overlap with the photon energy ranges found from the signatures of organic N compounds observed in the investigated micro- and nano-C repository environment. However, since inorganic N generally represents <5% of total N in mineral soils (Schulten and Schnitzer, 1998), it is highly unlikely that the N K-edge spectra of this microbial organic N enriched hotspot could be considerably influenced by the signals from mineral N to the point that they could be too relevant for the interpretation of the N K-edge NEXAFS spectra of the investigated micro- and nano-C repository environment.

3.3. Ca L-edge STXM-NEXAFS spectromicroscopy

Similar to the C and N-Kedge NEXAFS spectromicroscopy micrographs, the Ca L-edge target map (Fig. 4b) showed detailed morphological features of the filament-like organic structure (light gray) and the nearby organomineral interface (dark red) regions. The Ca L-edge cluster indices map (Fig. 3c) clearly revealed the nano-scale spatial distribution of the various Ca compounds and the respective spectral signatures found at the inner, intermediate and outer regions of the filament-like structure (Fig. 4m), and the organomineral interface (Fig. 4n). The Ca L-edge NEXAFS spectral features (Fig. 4m and n) were generally limited to a narrow energy range between 346.9 eV and 352.3 eV. However, they exhibited a rich and complex Ca fine edge structure present in the investigated micro- and nano-C repository environment.

3.3.1. Cluster analysis of Ca from the filament-like structure

The Ca L-edge spectral features collected from the inner, intermediate and outer regions of the filament-like structure (Fig. 4m) revealed four principal features, where the two main spin-orbit related peaks i.e., L₃ 2P_{3/2} and L₂ 2P_{1/2} appearing near 349.1 eV and 352.2 eV, respectively, along with smaller crystal field L₃ 2P_{3/2} and

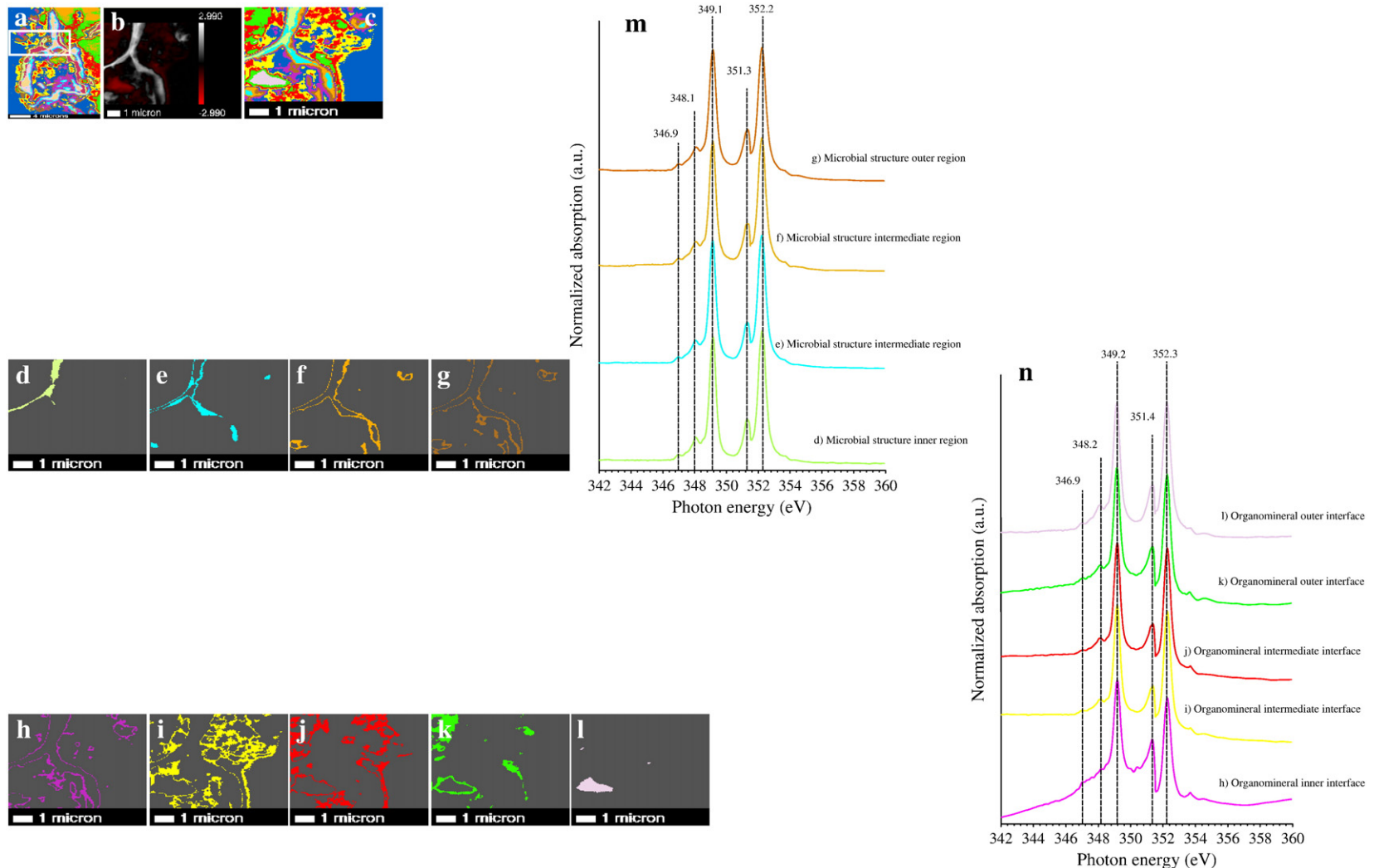


Fig. 4. High resolution C K-edge cluster indices map showing the region where Ca analysis was conducted (panel a), Ca L-edge NEXAFS target (panel b) and cluster indices (panel c) maps and individual Ca NEXAFS cluster images of the various regions of the filament-like structure (panels d–g) and the nearby organomineral interface (panels h–l), and their respective spectra (panels m and n).

L_2 $2P_{1/2}$ peaks near 348.1 eV and 351.3 eV preceding the main L_3 and L_2 peaks, respectively. Additionally, a small L_3 leading peak near 346.9 eV was observed in the spectral features of the strand-like microbial structure (Fig. 4m). Measurements of the energy separation of the main (L_2 $2P_{1/2}$ - L_3 $2P_{3/2}$) and the smaller (L_2 $2P_{1/2}$ - L_3 $2P_{3/2}$) Ca L_2 and L_3 edges of these spectra were between 3.0 eV and 3.1 eV and 3.2 eV and 3.2 eV, respectively. These values were generally inline with the 2p spin-orbit splitting of Ca metal determined experimentally for a variety of Ca standards by Fleet and Liu (2009). Naftel et al. (2001) indicated that the origin of these multi-peak patterns is known to be the crystal field arising from the symmetry of the atoms surrounding the Ca^{2+} ion in the first co-ordination sphere. Benzerara et al. (2004) pointed out that microbes are often associated with Ca-containing minerals. Calcium ion (Ca^{2+}) is also known to act as a cation bridge between negatively charged functional groups including extracellular polymeric substances on microbial surface (Hitchcock et al., 2009). Accordingly, the two well-resolved spectral features corresponding to the main L_3 (349.1 eV) and L_2 (352.3 eV) Ca L-edge peaks (Fig. 4m) could be the results of various Ca phosphate compounds (Naftel et al., 2001; Cailleau et al., 2005; Fleet and Liu, 2009; Obst et al., 2009). The major L_3 $2P_{3/2}$ (near 349.1 eV) and L_2 $2P_{1/2}$ (near 352.2 eV) absorption bands and the smaller L_3 (346.9 eV and 348.1 eV) and L_2 (351.3 eV) peaks could also arise from Ca associated with exoenzymes such as amylases and proteases, from Ca-containing organophosphates compounds such as Ca glycerophosphate ($HOCH_2CH(OH)CH_2OPO_3Ca$) or even from low molecular weight organic acids such as oxalates produced by soils fungi and known to interact particularly with metal ions such as Ca forming polymorphs of Ca oxalate (e.g., weddellite, $CaC_2O_4 \cdot 2H_2O$ and whewellite, $CaC_2O_4 \cdot H_2O$) (Naftel et al., 2001; Huang and Germida, 2002; Cailleau et al., 2005). This could be due to the fact that phosphorus is an important constituent of microbial nucleic acids and phospholipids, a result in agreement with both C and N K-edge NEXAFS investigations of this micro- and nano-C repository environment. Lengeler et al. (1999) indicated that some commonly found species of soil bacteria use low molecular weight organic acids as their sole source of C and energy through the tricarboxylic acid and glyoxylate cycles. Cailleau et al. (2005) also pointed that despite the low solubility of Ca oxalate, it can be dissolved by oxalate-utilizing bacteria. Although the general metabolic role of oxalates in microorganisms remains unclear, it is generally believed that they can be used by some soil bacteria for regulating pH, and Al detoxification (Tanner and Bornemann, 2000).

3.3.2. Cluster analysis of Ca from the organomineral interface

The most evident feature of the Ca $L_{3,2}$ -edge NEXAFS spectra collected from the organomineral interface (Fig. 4h–l) in the vicinity of the strand-like nano-repository zone was the splitting of the two principal edge peaks, giving rise to two relatively intense doublets appearing near the main L_3 $2P_{3/2}$ (349.2 eV) and L_2 $2P_{1/2}$ (352.3 eV) peaks (Fig. 4n). Qualitative comparison of the spectral features of the organomineral interface regions also indicated that although both L_3 and L_2 crystal field spectra were present, the smaller crystal field L_3 $2P_{3/2}$ (near 348.2 eV) peaks seem to be less developed than the more pronounced L_2 $2P_{1/2}$ (near 351.4 eV) peaks. Politi et al. (2008) demonstrated that the absence or appearance of less intense L_3 and L_2 crystal field peaks closer to the main L_3 and L_2 peaks, where they appear as shoulders, in the Ca absorption line-shapes is an indication for the presence of disordered or amorphous forms of Ca carbonate structures, while the splitting of the main L_3 and L_2 peaks and appearance of a more pronounced and equally intense L_3 and L_2 crystal fields peaks is an indication of the well developed crystalline Ca phase structures. Therefore, it is possible to suggest that our Ca $L_{3,2}$ -edge NEXAFS spectra seem to indicate that amorphous Ca compounds are largely absent from the organomineral interface region present nearby the strand-like structure. In addition,

inorganic Ca compounds present in association with the microbial organic matter in the organomineral complex might be composed of mixtures of more transient and crystalline phases of Ca compounds such as dibasic Ca phosphate ($CaHPO_4$), tricalcium Ca phosphate ($Ca_3(PO_4)_2$) hydroxylapatite ($Ca_5(PO_4)_3(OH)$) and carbonate-hydroxylapatite ($Ca_5(PO_4,CO_3)_3(OH)$), where the carbonate group might be incorporated into the hydroxyapatite structure by substitution for phosphate groups and to a lesser extent by OH-ions, but not as part of Ca carbonates such as calcite ($CaCO_3$) or dolomite ($CaMg(CO_3)_2$) (Naftel et al., 2001; Cailleau et al., 2005; Sato et al., 2005; Fleet and Liu, 2009; Obst et al., 2009). The diminished role of $CaCO_3$ compounds in the organomineral interface near the filament-like structure might be attributed to the fact that, although soil micro-organisms have a potential to modify the pH of their surroundings to a more localized alkaline environment even in acid soil (Tanner and Bornemann, 2000; Cailleau et al., 2005), the pH of the investigated soil ($pH=5.3$) might not support accumulation of appreciable amount of $CaCO_3$ compounds (the stable pH for calcite is ~8.4; Cailleau et al., 2005). This suggestion is also supported by the results of the C K-edge NEXAFS spectra of this region, which clearly showed absence of observable peaks related to $CaCO_3$ structures. The presence of Ca phosphates in the organomineral interface seem to be important in the preservation of organic C in this micro- and nano-C repository environment, since its precipitation is credited to prevent the degradation of organic C compounds such as nucleic acids by nucleases released by bacterial cells (Benzerara et al., 2004). These authors also observed an intimate association between Ca phosphate compounds and organic biomolecule matrixes composed of proteins, extracellular polymeric substances such as exopolysaccharides and DNA molecules in and around bacterial cells. Although Ca^{2+} ions do not form strong coordination complexes with organic molecules in contrast to hydroxypolyations (Fe^{3+} and Al^{3+}), they are also known to bind to negatively charged functionalities originating from microbial polysaccharides with glucuronic-, galacturonic-, manuronnic-, pyruvic- and succinic-acid groups through polyvalent cation bridges (Lützow et al., 2006). Similar to the Ca chemistry of the strand-like structure, the Ca L-edge NEXAFS spectral signatures (Fig. 4n) from the various regions of the organomineral interface (Fig. 4h and l) could also be the results of Ca-bearing organic compounds such as glycerophosphate ($HOCH_2CH(OH)CH_2OPO_3Ca$) or from the most common forms of Ca oxalate ($CaC_2O_4 \cdot 2H_2O$ and $CaC_2O_4 \cdot H_2O$) compounds commonly encountered in soils (Naftel et al., 2001; Cailleau et al., 2005) originating possibly from microbial metabolites and sequestered in the investigated micro- and nano-organic C repository environment.

3.4. Fe L-edge STXM–NEXAFS spectromicroscopy

The spatially resolved Fe L-edge target map (Fig. 5b) clearly showed the filament-like structure (dark gray) and the nearby organomineral interface (light gray) regions in the investigated micro-organomineral assemblage. The Fe L-edge cluster indices map (Fig. 5c) revealed the nano-scale spatial distribution of the various Fe compounds and their spectral signatures at the inner, intermediate and outer regions of the filament-like structure (Fig. 5l), and the organomineral interface (Fig. 5m), where organic C present in intimate association with the mineral matter. Our results showed that the Fe L-edge NEXAFS spectra recorded from the investigated micro-organomineral assemblage have two distinct absorption band regions. The first region was approximately between 706.0 and 715.0 eV; and represents an electronic dipole transition between $2p_{3/2}$ and 3d orbitals, also called the L_3 edge, while the second region also called the L_2 edge was located roughly between 720 and 728 eV, and implies an electronic transition between $2p_{1/2}$ and 3d orbitals (Van derlaan and Kirkman, 1992).

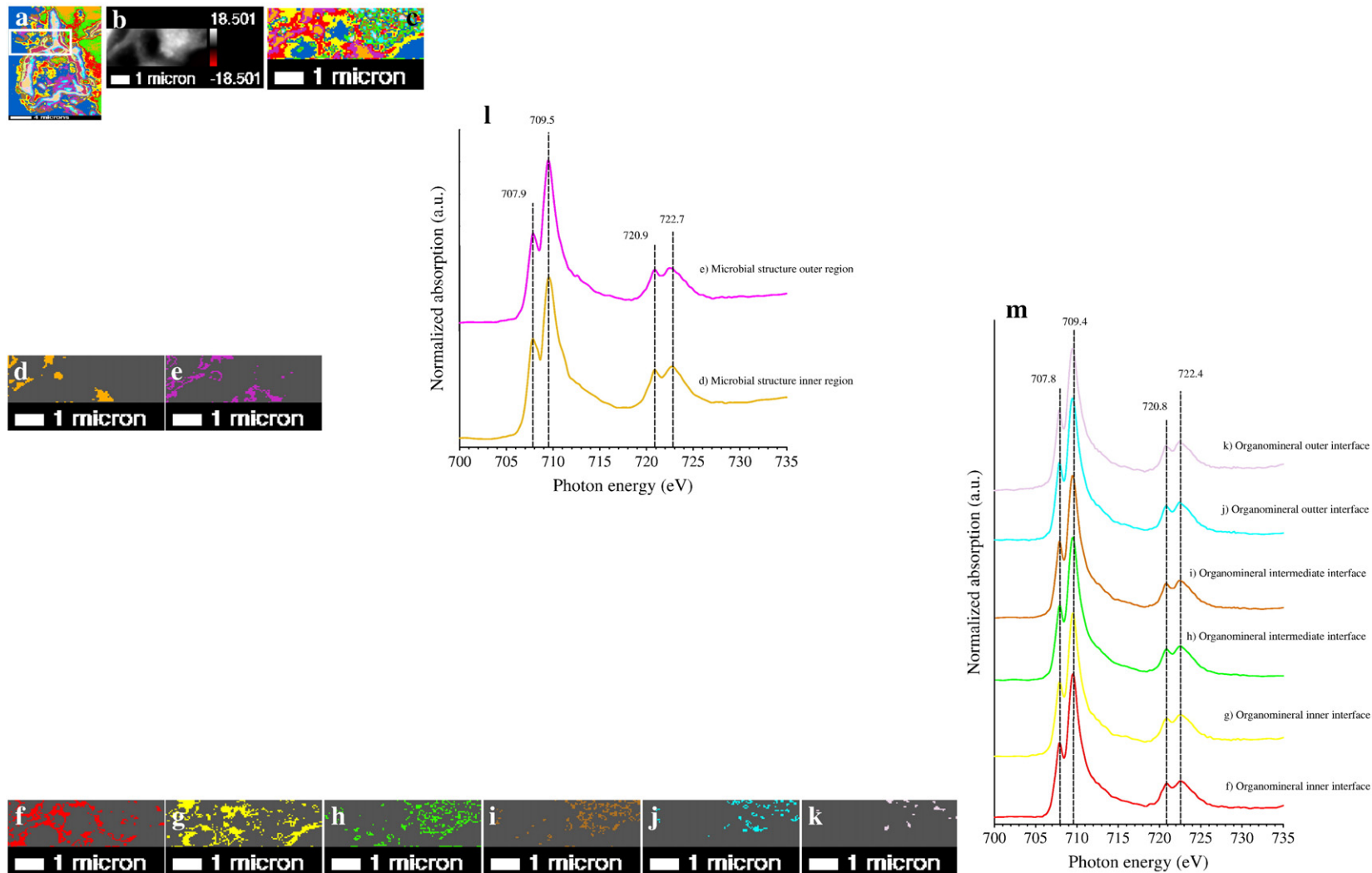


Fig. 5. High resolution C K-edge cluster indices map showing the region where Fe analysis was conducted (panel a), Fe L-edge NEXAFS target (panel b) and cluster indices (panel c) maps and individual Fe NEXAFS cluster images of the various regions of the filament-like structure (panels d–e) and the nearby organomineral interface (panels f–k), and their respective spectra (panels l and m).

3.4.1. Cluster analysis of Fe from the filament-like structure

The Fe L-edge spectra (Fig. 5l) determined from Fe 2p cluster maps showing the inner (Fig. 5d) and outer (Fig. 5f) regions of the filament-like structure exhibited multiple peaks at the iron L₃- (near 707.9 eV and 709.5 eV) and L₂- (near 720.9 and 722.7 eV) edges. The Fe L-edge NEXAFS spectra also show that both the L₃- and L₂-edge resonances were characterized by clearly separated and well-resolved doublets. However, the Fe L₃ 2P_{3/2} peaks were generally less pronounced compared to the sharp and more intense Fe L₃ 2P_{3/2} peaks, which appeared near 709.5 eV (Fig. 5l). In contrast, the Fe L₂ 2P_{1/2} transitions that appeared near 720.9 and 722.7 eV were somewhat broader and of equal magnitude in their intensity. Dynes et al. (2006) and Hitchcock et al. (2009) indicated that the oxidation state of Fe can be determined from the shape of these Fe 2P_{3/2} peaks signals, the peak position and relative intensities of the two peaks. These authors reported that although both Fe²⁺ and Fe³⁺ compounds show double peaked Fe L₃ 2P_{3/2} signal, the L₃ 2P_{3/2} bands originating from Fe²⁺ rich species generally start at lower energy compared the ones originating from Fe³⁺ rich species (van Aken and Liebscher, 2002). In addition, other investigations involving oxidation states of iron in mineral standards also showed that systems dominated by the divalent iron form display a sharp Fe 2p_{3/2} absorption peak near 708.0 eV, followed by a less intense peak near 710.0 eV, while matrices rich in trivalent iron show a less intense peak around 708.0 eV, followed by a very intense resonance near 709.5 eV (van Aken et al., 1998; van Aken and Liebscher, 2002; Majestic et al., 2007). Therefore, although the presence Fe²⁺ species cannot be fully excluded, based on the Fe L_{3,2}-edge NEXAFS spectra recorded from the filament-like structure, it is possible to suggest that the external and internal regions of the microbial structure present in the investigated micro- and nano-C repository environment seem to be dominated by trivalent iron rich species. This was also supported by the measured separation of the Fe L₃ and L₂ peak maxima (13.2 eV and 13.0 eV for the inner and outer regions, respectively) of the strand-like structure, which arises due to spin-orbit splitting of the Fe³⁺ and Fe²⁺ species, values very much in line with the results (13.0 eV for Fe³⁺ and 12.9 eV for Fe²⁺) reported by van Aken and Liebscher (2002) for a variety of Fe-containing compounds. Similar results were reported by Hitchcock et al. (2009), where filamentous bacteria accumulated mainly the Fe³⁺ species, and only a small proportion of iron was composed of divalent iron species. Hunter et al. (2008) also indicated that the Fe³⁺ species of iron are found to be predominantly associated with the bacterial cells, while the Fe²⁺ species were present at a much lower level in the extracellular milieu adjacent to the bacteria with strong trivalent iron levels. The possible sources of the Fe³⁺ iron forms in the internal and external surfaces of the strand-like structure could vary from sorption of soluble or colloidal Fe³⁺ iron-containing species, as ferric iron is known to bind tenaciously to bacterial surfaces, to oxidation of cell-bound Fe²⁺ iron species (Chan et al., 2004; Châtellier et al., 2004; Hitchcock et al., 2009). Other sources of Fe³⁺ iron in the filament-like structure could also include siderophores, secondary low-molecular-mass coordination high-affinity iron chelating compounds rich in carboxylate, phenolate, catecholate and hexamate moieties produced and exuded by a wide variety of fungi and bacteria (Neilands, 1995; Schröder et al., 2003; Miethke and Marahiel, 2007). They are highly specific Fe³⁺ ligands; and interact with iron oxides and hydroxide mineral phases and form soluble Fe³⁺ complexes making this iron species either accessible for reduction and/or for cellular uptake and assimilation by microorganisms (Schröder et al., 2003). Dong (2010) and Gadd (2010) also reported that microbial cell walls, outer layers, and exopolymers can sorb, bind or entrap many of the soluble and insoluble iron species, as this metal is known to be an important component of cytochromes, ferredoxins and present as a cofactor of enzymes such as dehydratases in soil microorganisms (Huang and Germida, 2002).

3.4.2. Cluster analysis of Fe from the organomineral interface

The Fe L_{3,2}-edge spectral features (Fig. 5m) collected from the organomineral interface (Fig. 5f–k) near the stand-like structure revealed intense and well-resolved double peak Fe L₃ 2p_{3/2} signals near 707.8 eV and 709.4 eV and additional two Fe L₂ 2p_{1/2} peaks near 720.8 eV and 722.4 eV. The Fe L_{3,2}-edge spectral features and peak positions from the organomineral interface were remarkably similar to the Fe 2p NEXAFS spectral signatures observed from resonances of hematite, (α -Fe₂O₃), goethite (α -FeO(OH)), ferrihydrite (Fe₅HO₈·4H₂O), schwertmannite (Fe₃O₈(OH)₆(SO₄)), and magnetite (Fe₃O₄) (van Aken and Liebscher, 2002; Xiong et al., 2009). However, these Fe L_{3,2}-edge features were distinctly different from spectral signatures observed from minerals composed exclusively of ferrous (Fe²⁺) iron such as wüstite (FeO), and hercynite (FeAl₂O₄) (Crocombette et al., 1995; van Aken and Liebscher, 2002). These results are clear indication that the investigate metal-rich micro- and nano-C repository environment appeared to be predominantly composed of more crystalline iron (Fe³⁺) oxides (e.g. hematite) and iron (Fe³⁺) oxyhydroxides (e.g. goethite), as well as less crystalline iron (Fe³⁺) hydroxide (Fe(OH)₃) and oxyhydroxides (e.g. ferrihydrite) species and Fe³⁺ cations. Our results are inline with the results of Violante et al. (2002), who suggested that various polymorphs of FeO(OH) and Fe₂O₃ commonly known to coexist as end products of advanced weathering in many tropical soils, where leaching is strong and the soil is more acidic. Iron compounds are commonly released in the soil by weathering as less ordered iron (III) hydroxides (Fe(OH)₃) in oxidizing situations and as dissolved iron (II) hydroxides (Fe(OH)₂) in reduced conditions. These compounds will eventually dehydrate and crystallize as hematite or goethite. Hematite formation tends to be favored in the warm environments, while goethite is more stable in humid and cooler environments. The presence of a more oxidized ferric (Fe³⁺) iron oxide and hydroxide species in the investigated organomineral interface was, therefore, in keeping with the warm, well aerated, and lower pH environment of the studied soils. Iron oxides, hydroxides, and oxyhydroxides (FeOx) are generally known to influence soil organic matter stabilization, as evidenced by positive correlations between metal and total organic C concentrations among a range of soils (Tiessen et al., 1984; Skjemstad et al., 1989; Kaiser and Guggenberger, 2000). Thus, the presence of various oxides, hydroxides, and oxyhydroxides of Fe in the inner, intermediate and outer regions of the organomineral interface is critical for organic C stabilization; because these oxides, hydroxides and oxyhydroxides could provide vast sorbent surface area or could also coat clay and create a variety of mineral surface types in the organomineral interface (Kleber et al., 2007). Sollins et al. (1996) indicated that the bonding mechanism between the mineral surfaces and the organic C could differ depending on the nature of the sorbate and sorbent present in the localized geochemical micro-scale environments, and suggested that several mechanisms could play a role in the stabilization of C in the organomineral complex. Therefore, one of the possible mechanisms for the observed association of organic C with the mineral matter in the investigated micro- and nano-C repository environment could be due to sorption of negatively charged organic C (e.g., dissociated carboxylic (COO⁻) acid and phenolic (OH⁻) groups observed in the investigated organomineral interface by C K-edge NEXAFS spectroscopy) through replacement of surface hydroxyl groups (ligand exchange). Gu et al. (1994) and Lützow et al. (2006) stated that such anion exchange between simple coordinated OH groups on mineral surfaces and carboxyl and phenolic groups of organic matter is one of the most important mechanism for the formation of strong (e.g. Fe–O–C bonds) organomineral associations, especially in acid soils rich in minerals with protonated hydroxyl groups. Although, organic anions are normally repelled from negatively charged surfaces of the exchange complex, the trivalent iron (Fe³⁺) present in the organomineral interface of the investigated micro- and nano-C repository environment could also serve as a polyvalent cation bridge

binding together the negatively charged surfaces of the clay minerals and the acidic functional groups of organic C. Microbially secreted polysaccharides frequently carry negative charge due to the presence of uronic acids that adsorb strongly to negatively charged clay surfaces through polyvalent cation bridging involving iron (Chenu, 1995). Thus, complexation reactions involving such organic C compounds and structural cations of edges or Fe cations released from primary and secondary hydroxyl iron coatings on clay colloids could be additional possible binding mechanisms for the intimate association observed between organic C and Fe compounds in the organomineral interface (Huang, 2004). These suggestions are supported by the results of Schwertmann et al. (1986), who reported that complexation of Fe(III) ions with dissociated functional groups on organic matter can occur in soil micro-environments with high supply of iron III and decomposed and humified materials. Petersen (1976) and Wada (1995) reported that precipitation of these complexes is an important stabilization mechanism in volcanic and acid leached subsurface soils. Physical protection of organic C via microaggregation induced by metal oxides (especially FeOx) could also be another possible mechanism for the stabilization of organic C in this micro- and nano-C repository environment. The importance of FeOx for organic matter stabilization in soil aggregates has been shown in tropical soils by Shang and Tiessen (1998). These results seem to provide further evidence to our suggestion that given the complex compositional chemistry of the organic sorbate observed using C and N NEXAFS, the diverse nature of the mineral sorbent observed with Fe NEXAFS, and the variety of mechanisms that these organic C species could interact with the surfaces of the soil mineral interface, no single process seem to be the dominant mechanism for the adsorption of microbial C to the mineral matter, and its subsequent sequestration in the investigated micro- and nano-C repository environment.

3.5. Al K-edge STXM–NEXAFS spectromicroscopy

The Al K-edge target map (Fig. 6b) showed the filament-like organic structure (light gray) and the nearby organomineral interface (dark red) region in the investigated organomineral assemblage. The Al K-edge cluster indices map (Fig. 6c) illustrated the micro- and nano-scale spatial distribution of Al compounds (Fig. 6d–i) and their signatures at the exterior and interior regions of the filament-like structure (Fig. 6j), and the organomineral interface (Fig. 6k). The Al spectral signatures were well-resolved and distinct features of this metal appeared within the energy range of 1565.4–1588.5 eV providing a clear indication for the presence of rich fine structural features related to Al in the investigated organomineral assemblage. Shaw et al. (2009) indicated that these Al 1s NEXAFS absorption features arise from transitions of core electrons to the first empty bound states (1s–3p) and from multiple scattering inside the nearest neighbor coordination shell or among the first neighbors. Ildefonse et al. (1998), Doyle et al. (1999) and Hu et al. (2008) reported that Al K-edge NEXAFS can be diagnostic for probing the bonding and symmetry of the local coordination environment around Al atoms and could be employed to identify Al compounds in complex environmental samples. Hu et al. (2008) showed that Al K-edge NEXAFS is particularly powerful in differentiating four- and six-fold coordination environments.

3.5.1. Cluster analysis of Al from the filament-like structure

The Al K-edge cluster maps from the exterior (Fig. 6d) and interior (Fig. 6e) regions of the filament-like structure showed that, unlike the distribution of C, N, Ca and Fe that occurred in a more discrete manner, the nano-scale distribution of Al appeared to be in a more dispersed fashion. The Al 1s spectral features (Fig. 6j) recorded from the exterior (Fig. 6d) and interior (Fig. 6e) regions of the filament-like structure exhibited multiple peaks with the two main features near 1565.4 eV and 1567.6 eV, while additional peaks near

1578.5 eV, 1582.5 eV, and 1588.5 eV, with a shoulder appearing near 1569.7 eV. These spectral features and energy positions were largely similar to the spectra collected from gibbsite (α -Al(OH)₃), kaolinite ($\text{Al}_4(\text{Si}_4\text{O}_{10})(\text{OH})_8$) and Al-goethite ($\text{Fe}_{1-x}\text{Al}_x\text{OOH}$) (Li et al., 1995a; Ildefonse et al., 1998; Hu et al., 2008; Shaw et al., 2009). Yoon et al. (2004) demonstrated that bacterial cells can form close association with aluminum oxides and phyllosilicate clays, and form bacteria-mineral aggregates via adhesive action of extracellular polysaccharides. Similarly, Ehrlich (2002) stated that mineral particles commonly adhere to microbial cell surfaces through the hydrophilic nature of the exopolymer produced by soil microorganisms or via hydrophobic cell surface structures, if the mineral surface is hydrophobic. Hydrophilic attachments may involve electrostatic interactions between negative charges at the cell surface or exopolymers surrounding the cell and positively charged regions at the mineral surface.

3.5.2. Cluster analysis of Al from the organomineral interface

The Al K-edge spectra (Fig. 6k) recorded from the organomineral interface revealed three distinct main features near 1565.3 eV, 1566.8 eV, and 1567.8 eV, followed by a shoulder near 1569.9 eV. Additional peaks were observed near 1574.5 eV, 1578.5 eV, 1582.5 eV and 1588.5 eV. These spectral features and energy positions were largely similar to the spectra collected from Al-containing crystalline standard compounds with six-fold coordinated Al in dioctahedron layer such as kaolinite and gibbsite, as well as from less differentiated low Al concentrations Al-goethite formed by replacement of Fe by Al atoms in goethite (Li et al., 1995a; Ildefonse et al., 1998; Hu et al., 2008; Shaw et al., 2009). However, with the exception of gamma alumina (γ -Al₂O₃) and illite ((MgCaK)_{1.52}Al₄(SiAl)₄O₂₀(OH)₄) where we observed a slight resemblance, the spectra collected from the organomineral interface did not exhibit signatures related to Al compounds with four-fold Al such as albite (NaAlSi₃O₈), six-fold Al in octahedron layer such as corundum (α -Al₂O₃), and diaspore (α -AlO(OH)) and to Al compounds with mixed (four- five- and six-fold Al) coordination number such as muscovite, $\text{KAl}_2(\text{Si}_3\text{Al})\text{O}_{10}(\text{OH})_2$ and smectite (CaNaH)(AlMgFeZn)₂(SiAl)₄O₁₀(OH)_{2-x}H₂O) (Ildefonse et al., 1998; Hu et al., 2008; Shaw et al., 2009). Based on these results it is possible to suggest that the possible source of the various Al-containing compounds in the investigated organomineral interface could range from aluminum hydroxide polymorphs such as gibbsite, phyllosilicate clays such as kaolinite (to a lesser extent illite) to aluminous goethite or other Al-containing minerals with a similar local environment of the Al atom to that of these minerals. Kaolinite, the most common of the 1:1 silicate clay minerals with a hydrophobic siloxane surface, is an important component of many soils especially those that are found in warm and humid tropical environments and subjected to intensive weathering. With the help of proteinaceous compounds, which serve as a surface conditioner that adds polar functionality to its low-charge siloxane surfaces, kaolinite have been implicated as an important clay mineral for organic C stabilization (Kleber et al., 2007). Polymorphs of Al hydroxides are also common products of weathering of soils in tropical and subtropical environments; and they are known to be among the most major minerals in many Oxisols and Ultisols. Our investigation provided a clear evidence that various phases of Al-containing oxides, hydroxides and oxyhydroxides could coexist together with the polymorphs of FeO(OH), Fe₂O₃ and silicate clays such as kaolinite supporting the suggestions of Violante et al. (2002). The observed coexistence have a practical significance in stabilization of organic C in the investigated organomineral interface, since these minerals are excellent sources of polyvalent cations such as Al³⁺, Al hydroxyl and Al oxyhydroxy surface groups and edge sites on clay minerals, which can attract and bind microbial biopolymers such as proteins, nucleic acids and polysaccharides identified by C and N NEXAFS

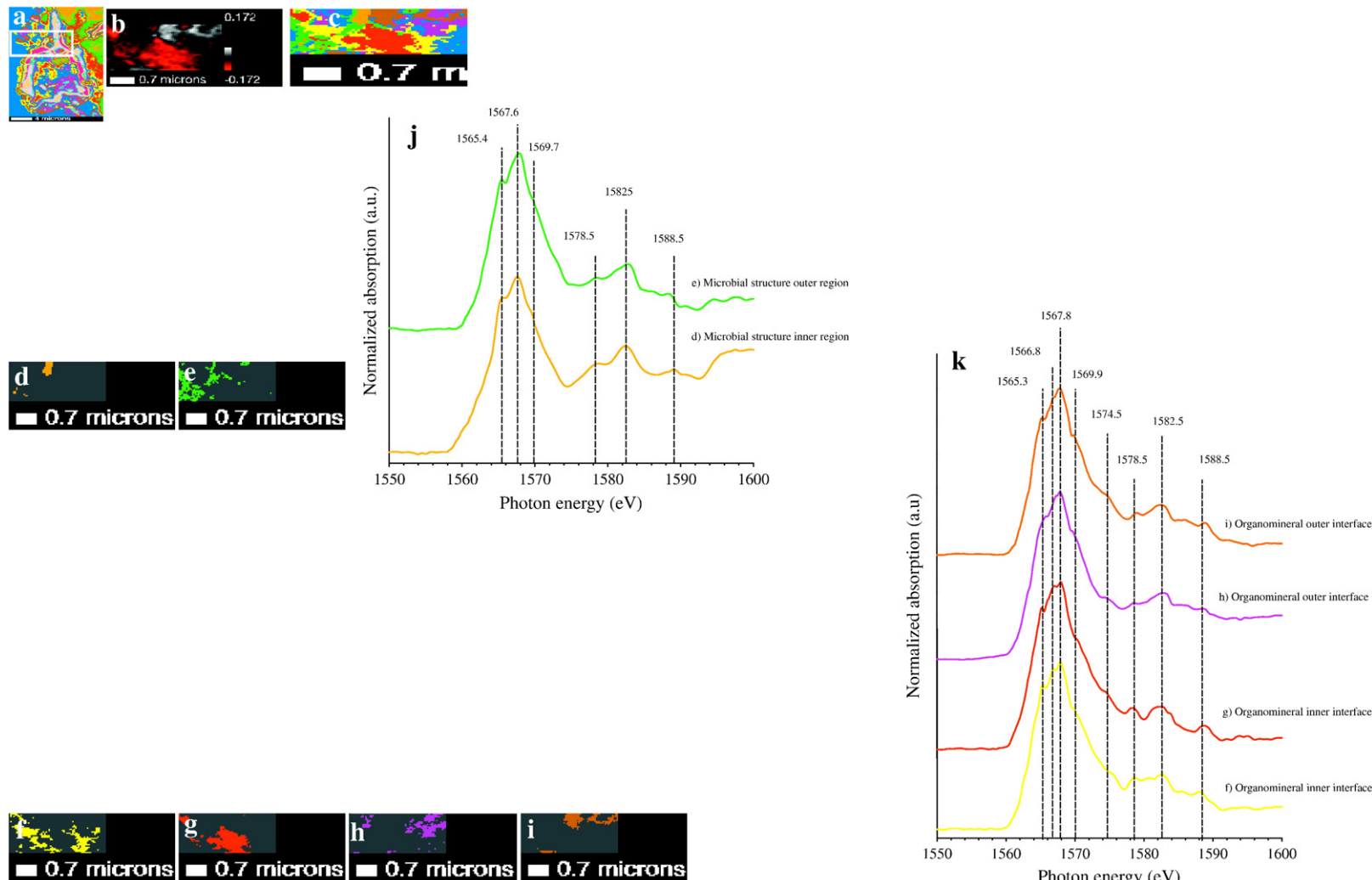


Fig. 6. High resolution C K-edge cluster indices map showing the region where Al analysis was conducted (panel a), Al K-edge NEXAFS target (panel b) and cluster indices (panel c) maps and individual Al NEXAFS cluster images of the various regions of the filament-like structure (panels d–e) and the nearby organomineral interface (panels f–i), and their respective spectra (panels j and k).

from the submicron-C repository environment and known to contain negatively charged carboxylic, phenolic, enolic, thiolate and phosphate functionalities. These organic moieties could bind to the mineral surfaces through a variety of binding mechanisms ranging from ligand exchange, polyvalent cation bridges, and weak interactions such as hydrophobic interactions, van der Waals forces and H-bonding (Theng, 1979; Huang, 2004). Chenu and Stotzky (2002) and Stotzky (2002) suggest that the adsorption of these organic molecules to mineral surfaces at times can be considered non-reversible, since it can result in conformational changes that render the biomolecules unavailable to the action of extracellular enzymes. The inhibitory effects of Al (and to a lesser extent Fe) on soil respiration and its subsequent role in accumulation of soil organic C observed in numerous field and laboratory studies have been also described by Tyler et al. (1989) and Giller et al. (1998). Although, the effect of Al ion cannot be often separated from its ability to form cation bridges, Al is also among the various metal ions (e.g., Fe and Ca) that could potentially stabilize soil organic C through complexation reactions (Lützow et al., 2006). For example, Jones et al. (2001) clearly showed that Al-complexes of citrate and oxalate in soils were much more stable in comparison with the free citrate and oxalate compounds. Biomolecules released from microbial activity are also known to interact with Al-containing compound in soils and promote transformation of poorly ordered and highly reactive intermediate phases of Al oxyhydroxides to more stable crystalline Al hydroxides by a series of perturbing organic ligands such as aspartic, tannic, malic and citric acids (Hu et al., 2008). Torn et al. (1997) indicated that poorly ordered and highly reactive Al oxyhydroxides are particularly important for the stabilization and biogeochemical cycling of C in soils.

3.6. Si K-edge STXM–NEXAFS spectromicroscopy

The spatially resolved Si K-edge target map (Fig. 7b) showed the strand-like organic structure (light gray) and the nearby organomineral interface (dark red) regions of the investigated micro-organomineral assemblage. The Si K-edge cluster indices map (Fig. 7c) illustrated the submicron spatial distribution of Si and the spectral signatures associated with the inner and outer regions of the filament-like structure (Fig. 7j) and the organomineral interface (Fig. 7k). The Si K-edge resonances from the filament-like structure and the nearby organomineral interface regions appeared to be well-resolved and within the energy range of 1842.3 and 1860.8 eV (Fig. 7j and k) in the Si 1s continuum suggesting the presence of rich fine structural features related to Si in this micro- and nano-C repository environment. The results of our Si K-edge NEXAFS spectra are similar to the values reported for the Si 1s spectra recorded from various Si-containing minerals by Seifert et al. (1996) and Urquhart et al. (1997). Hitchcock et al. (2009) stated that the 1s-edge absorption spectra of Si compounds have different shapes; and the position of the absorption maximum of Si-containing compounds is dependent not only on the oxidation state of Si (the net $\text{Si}^0\text{--Si}^{4+}$ shift is ~8 eV), but also on the coordination number, polymerization of SiO_4^{4-} , Si–O bond distance, Si–O bond valence, distortion of SiO_4^{4-} -tetrahedra, and the chemical substitution in both tetrahedral and octahedral sites of the silicate mineral (Li et al., 1993, 1995b; Urquhart et al., 1997). Li et al. (1993, 1995b), and Shaw et al. (2009) reported that the strong main Si K-edge peak, which in the present experiment correspond to peaks near 1842.3 eV (Fig. 7j and k) is related to the transition of Si 1s electrons to 3p-like (1s-3p) state. Peaks that appeared near 1845.7 eV and 1852.6 eV are due to the multiple scattering effect from more distant atom shells, while the resonances near 1847.3 eV and 1860.8 eV are contributions from the transitions of Si 1s electrons and characterized by the empty Si 3d (1s-3d) states or sometimes called symmetry-forbidden shape resonances (Li et al., 1993, 1995b).

3.6.1. Cluster analysis of Si from the filament-like structure

The Si K-edge cluster maps showed the nano-scale distribution of Si at the inner (Fig. 7d) and outer (Fig. 7f) regions of the filament-like structure. The Si 1s spectral features corresponding to regions of the strand-like microbial structure (Fig. 7j) exhibited multiple peaks with the high intensity main feature appearing near 1842.3 eV, while additional peaks were observed near 1845.7 eV, 1847.3 eV 1852.6 eV, 1857.7 eV and 1860.7 eV. These spectral features resemble the Si K-edge spectra collected from Si-containing phyllosilicate minerals such as kaolinite ($\text{Al}_4(\text{Si}_4\text{O}_{10})(\text{OH})_8$), pyrophyllite ($\text{Al}_2(\text{Si}_3\text{O}_{10})(\text{OH})_2$), illite ($(\text{MgCaK})_{1.52}\text{Al}_4(\text{SiAl})_4\text{O}_{20}(\text{OH})_4$) and biotite ($(\text{K}(\text{Mg}, \text{Fe})_3(\text{AlSi}_3\text{O}_{10})(\text{OH})_2$), as well as from tectosilicate minerals such as α -quartz (SiO_2) and microcline ($\text{K}(\text{AlSi}_3\text{O}_8)$) (Li et al., 1993, 1995b; Gilbert et al., 2003; Shaw et al., 2009). The results seem to suggest that these Si-containing minerals were present in possible association with the organic C functionalities present on the surface and immediate surroundings of the filament-like structure, and supplement the results from our Al NEXAFS spectroscopy. The presence of Si-containing compounds such as quartz in association with bacterial biofilms has been also reported by Urrutia and Beveridge (1994) and Hitchcock et al. (2009). These authors indicated that the majority of the signal detected from the filamentous bacteria and its immediate surrounding were associated with the organosilicate species in a C–O–Si bond. Heterogeneous attachment of Si onto bacterial surface organic C functional groups via hydrogen bonding, bonding to the positively charged functional groups and cation bridging was attributed by Urrutia and Beveridge (1994) and Hitchcock et al. (2009) for the observed binding of Si on the external surface of microorganisms. Since Si is often associated with Fe and Al oxides and hydroxides in the environment, Konhauser and Urrutia (1999) suggested that Fe sorbs to the bacterial surfaces followed by Si and Al sorption, a mechanism that could be relevant to this study. Heterogeneous silicate mineral and Fe oxide attachments to cell surfaces due to heterogeneous distribution of organic C functional groups on cell surfaces have been also reported by Dong (2010).

3.6.2. Cluster analysis of Si from the organomineral interface

The Si K-edge spectra (Fig. 7k) collected from the inner and outer regions of the organomineral interface (Fig. 7g–i) revealed distinct and well-resolved Si 1s resonances near 1842.5 eV, 1845.8 eV, 1847.4 eV 1851.9 eV, 1857.8 eV and 1860.8 eV. These spectral features showed a great deal of resemblance to the Si K-edge spectra of phyllosilicates ($\text{Si}_4\text{O}_{10}^{4-}$ – Q^3) minerals such as kaolinite, pyrophyllite and illite, as well as from tectosilicates (SiO_2 – Q^4) minerals such as α -quartz (Li et al., 1993, 1995b; Shaw et al., 2009). These results seem to suggest that the Si-containing minerals present in the organomineral interface region were composed of mixed silicate clay minerals. The investigated organomineral interface seem to be primarily composed of hydrous aluminum phyllosilicates with 1:1 type clay mineral structure such as kaolinite produced mostly under more intense weathering of primary silicate minerals. In addition, there is also a possibility that some 2:1 type aluminum phyllosilicates clay minerals produced under intermediate weathering such as illite that are known to contain iron and magnesium and tectosilicates such as quartz could be present in smaller proportions in the investigated organomineral interface. Our results also seem to indicate that phyllosilicate minerals with 2:1 type clay mineral structures produced under mild weathering such as chlorite ($(\text{MgAlFe})_{12}(\text{SiAl})_8\text{O}_{20}(\text{OH})_{16}$) were largely absent in the organomineral interface region, since the Si K-edge spectral features recorded from these clay minerals are distinctively different from the Si 1s spectra collected from the investigated micro- and nano-C repository environment. These results are in agreement with the findings from our Fe L–Al K-edge NEXAFS spectroscopy. The presence of 1:1 hydrous aluminum phyllosilicates together with various Fe- and Al-containing 2:1 clay minerals, less ordered Fe and Al oxyhydroxide

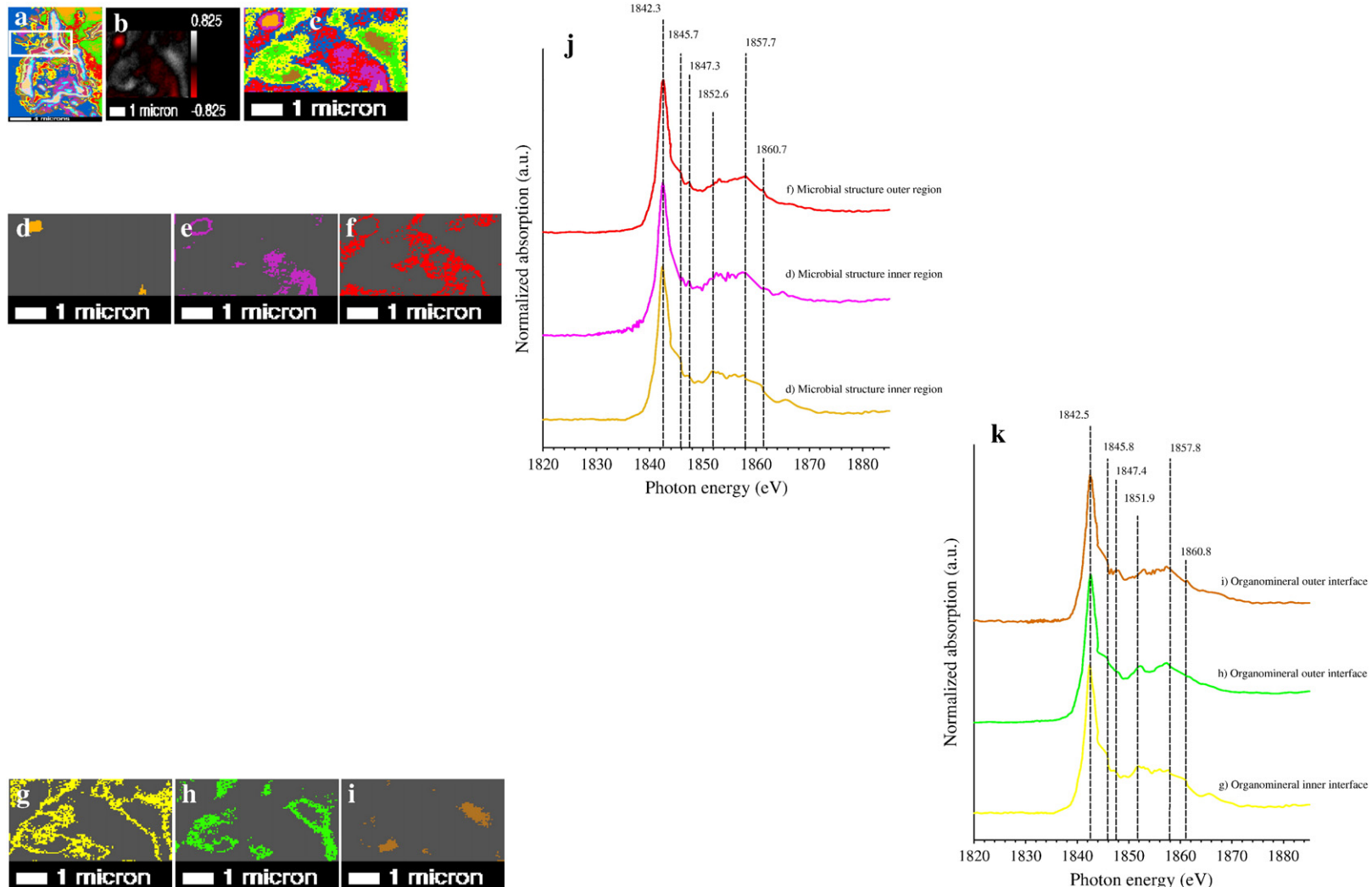


Fig. 7. High resolution C K-edge cluster indices map showing the region where Si analysis was conducted (panel a), Si K-edge NEXAFS target (panel b) and cluster indices (panel c) maps and individual Si NEXAFS cluster images of the various regions of the filament-like structure (panels d–f) and the nearby organomineral interface (panels g–i), and their respective spectra (panels j and k).

and more crystalline Fe and Al hydroxides that are the results of intensive weathering of Fe and Al containing primary silicate minerals could be an indication for the mixed layer or interstratified nature of the investigated organomineral interface; and may indicate the complexity of the matrix present in this submicron-C repository environment. The presence of interstratified matrix in organomineral interface is extremely important for binding and sequestering organic C, as it offers highly reactive lamellar and interlamellar layers and extensive variable and permanent charges, thus providing a driving force for the presence of various organic and inorganic cations and anions. [Violante et al. \(2002\)](#) indicated that short-range ordered Al precipitates and soluble OH-Al species often coat crystalline minerals in soils or interlayer into interlamellar spaces of phyllosilicates altering the surface properties of these clay minerals. [Huang \(2004\)](#) also stated that since the siloxane surface of 2:1 expandible layer silicates is negatively charged, the trigonal cavities of the surface of these silicate clay minerals can adsorb positively charged cations and polymers to form hydroxy-interlayered minerals in soils. These hydroxy-interlayered phyllosilicate clay minerals occur as single-structured or interstratified clay in soils throughout the world; although they tend to be more abundant in Oxisols, Ultisols and Alfisols present in warm tropical environments ([Violante et al., 2002](#); [Huang, 2004](#)). Because Fe and Al oxides are positively charged in the pH range of most soils (pH = 4.0–7.0), they are generally assumed to be the major sorbents of organic C in the organomineral interface ([Guggenberger and Haider, 2002](#)). However, since the edge sites of phyllosilicate clays could be amphoteric, these silicate minerals could also serve as an excellent binding and stabilization sites for polar organic C functionalities through a variety of binding mechanisms involving adsorption on external mineral surfaces, interlayer adsorption and metal cations occupying the exchange sites on the surface of silicate minerals ([Wershaw and Pinckney, 1980](#); [Guggenberger and Haider, 2002](#); [Huang, 2004](#); [Kleber et al., 2007](#)). The surfaces of phyllosilicate clay colloids could also complex with organics and form inner- and outer-sphere complexes with surface functional groups of minerals ([Huang, 2004](#)). This author further indicated that in the organomineral interface region, organic C molecules could interact with the surfaces of silicate clay colloids by a variety of mechanisms (e.g., ion exchange, protonation, hydrogen bonding, hydrophobic bonding on silicate clay-organic complexes, adsorption on external mineral surfaces and in silicate clay layers) based on the intrinsic nature and properties of the organic C species, the kind of exchangeable cation present on the surface of the clay colloid and the proportion of silicate minerals in the organomineral interface. Therefore, due to the mixed nature of phyllosilicate clay minerals, as well as the compositional complexity of Ca-, Fe- and Al-containing compounds and organic C functionalities present in the investigated organomineral interface observed using C, N, Ca, Fe, Al and Si NEXAFS spectromicroscopy, it is possible to suggest that no single binding mechanism could be accountable for the stabilization of organic C in this region. The apparent sequestration of organic C in this seemingly terminal micro- and nano-C repository environment thus could be the cumulative result of heterogeneous binding mechanisms.

4. Summary and future considerations

This study demonstrated the potential of synchrotron-based non-invasive STXM-NEXAFS spectroscopy to access the K- and L-edges of biogeochemically relevant elements (C, N, Ca, Fe, Al, Si) for global C cycling and acquire a spatially defined, multi-element submicron-level information to investigate the geobiological associations involving C functionalities, minerals and polyvalent metal ions, as well as other interactive surficial and architectural features important for understanding C sequestration in micro- and nano-C repository environments of mineral soils. The C NEXAFS micrograph clearly demonstrated the fine-scale distribution of total C and the existence

of spatially distinct and seemingly terminal micro- and nano-C repository environments zones, where organic C was sequestered in apparent agglomeration. These submicron-C repository zones were only a few micrometers apart from each other; yet they were considerably different compositionally, where one was ostensibly pyrogenic in composition, while the other was dominated by filament-like microbial structure with strikingly similarity to the C 1s NEXAFS spectral signatures of C isolated from soil fungal and bacteria colonies. The biomolecular matrix present in intimate association with the mineral matter in the organomineral interface, and in and around the strand-like structure was highly complex. It was composed of relatively labile polysaccharides, amino sugars, amino acids, nucleic acids, as well as phospholipid fatty acid structures with polar and non-polar termini possibly released into this submicron-C repository environment as microbial exudates or as the product of the biological membrane lysis of dead microorganisms. The compositional chemistry of the inorganic matter in the organomineral interface region was also highly complex ranging from Ca, Fe and Al ions, Fe and Al oxides, hydroxides and oxyhydroxides to aluminum phyllosilicate minerals that could provide a variety of polyvalent cations, hydroxyl surface functional groups and edge sites on clay minerals that can attract and bind microbial biopolymers. Based on the tremendous variability and complexity of the organic C functionalities and the astounding coexistence of various inorganic components present in the investigated organomineral interface region, it is possible to suggest that no single binding mechanism could be accountable for the organic C stored in this submicron-C deposition zone. We speculate the apparent binding and sequestration of organic C in this micro- and nano-repository environment could be the cumulative result of physical protection of C via metal oxides induced microaggregation and the heterogeneous binding mechanisms ranging from ion exchange, protonation, hydrogen bonding, hydrophobic bonding on silicate clay-organic complexes, anion adsorption to adsorption on external mineral surfaces and in silicate clay layers depending on the inherent characteristics of the organic C species, the type of exchangeable cation on the surface of the clay colloids and the proportion of silicate minerals present in the organomineral interface. However, additional studies are warranted to extend the results of the present investigation to aggregates of soils from a wider range of mineralogy. Future investigations should exploit the diagnostic potential of C, N, Al and Si K-edge and Ca and Fe L-edge STXM-NEXAFS spectromicroscopy, and target 2–20 nm sized and iron and aluminum oxide, hydroxide and oxyhydroxide and phyllosilicates nanoparticles in submicron-C repository environments as systems of interest. Understanding the compositional chemistry, chemical state and electronic structures and properties of such particles and their association with C could provide unprecedented ability to investigate the different phases present in the organomineral interface of environmental matrices such as soils could help isolate specific organic C binding mechanisms and processes; and generate a wealth of new nano- and atomic-level information about organic and oxide communities and their association in the organomineral interface of mineral soils. Of particular interest for future research are long-term changes along mineralogical gradients developed during pedogenesis.

Acknowledgments

This study was financially supported in part by grants from Agriculture and Food Research Initiative Competitive Grant of the National Institute of Food and Agriculture (2008-35107-04511) and from the Geobiology and Low-Temperature Geochemistry Program of the National Science Foundation (EAR-0819689). The C K-edge NEXAFS spectromicroscopy measurements were recorded at X1A1 beamline of the National Synchrotron Light Source (NSLS), Brookhaven National Laboratory (BNL), using the STXM end station. The N, Al, Si K-edge, and Ca and Fe L-edge NEXAFS spectromicroscopy measurements

were performed using STXM end station at the soft X-ray spectromicroscopy (SM) 10ID-1 beamline of the Canadian Light Source (CLS).

References

- Ade, H., Urquhart, S.G., 2002. NEXAFS spectroscopy and microscopy of natural and synthetic polymers. In: Sham, T.K. (Ed.), *Chemical Applications of Synchrotron Radiation*. World Scientific Publishing, River Edge, NJ, pp. 285–355.
- Amelung, W., Kaiser, K., Kammerer, G., Sauer, G., 2002. Organic carbon at soil particle surfaces – evidence from X-ray photoelectron spectroscopy and surface abrasion. *Soil Science Society of America Journal* 66, 1526–1530.
- Baldock, J.A., Nelson, P.N., 2000. Soil organic matter. In: Sumner, M.K. (Ed.), *Handbook of Soil Science*. CRC Press, Boca Raton, FL, pp. B25–B84.
- Benzerara, K., Yoon, T.H., Tyliszczak, T., Constantz, B., Spormann, A.M., Brown, G., 2004. Scanning transmission X-ray microscopy study of microbial calcification. *Geobiology* 2, 249–259.
- Boese, J., Osanna, A., Jacobsen, C., Kirz, J., 1997. Carbon edge XANES spectroscopy of amino acids and peptides. *Journal of Electron Spectroscopy and Related Phenomena* 85, 9–15.
- Boyce, C., Cody, G., Feser, M., Jacobsen, C., Knoll, A., Wirick, S., 2002. Organic chemical differentiation within fossil plant cell walls detected with X-ray spectromicroscopy. *Geology* 30, 1039–1042.
- Brandes, J.A., Lee, C., Wakeham, S., Peterson, M., Jacobsen, C., Wirick, S., Cody, G.D., 2004. Examining marine particulate organic matter at sub-micron scales using scanning transmission X-ray microscopy and carbon X-ray absorption near edge structure spectroscopy. *Marine Chemistry* 92, 107–121.
- Brash, J.L., Horbett, T.A., 1995. Proteins at interfaces. An overview. In: Horbett, T.A., Brash, J.L. (Eds.), *Proteins at Interfaces II Fundamentals and Applications*. American Chemical Society, Washington, DC, pp. 1–25.
- Braun, A., Huggins, F.E., Shah, N., Chen, Y., Wirick, S., Mun, S.B., Jacobsen, C., Huffman, G.P., 2005. Advantages of soft X-ray absorption over TEM-ELS for solid carbon studies—a comparative study on diesel soot with EELS and NEXAFS. *Carbon* 43, 117–124.
- Braun, A., Mun, B.S., Huggins, F.E., Huffman, G.P., 2007. Carbon speciation of diesel exhaust and urban particulate matter NIST standard reference materials with C(1s) NEXAFS spectroscopy. *Environmental Science and Technology* 41, 173–178.
- Cailleau, G., Braissant, O., Dupraz, C., Aragno, M., Verrecchia, E.P., 2005. Biologically induced accumulations of CaCO₃ in orthox soils of Biga, Ivory Coast. *Catena* 59, 1–17.
- Chan, C.S., De Stasio, G., Welch, S.A., Girasole, M., Frazer, B.H., Nesterova, M.V., Fakra, S., Banfield, J.F., 2004. Microbial polysaccharides template assembly of nanocrystal fibers. *Science* 303, 1656–1658.
- Châtellier, X., West, M.M., Rose, J., Fortin, D., Leppard, G.G., Ferris, F.G., 2004. Characterization of iron-oxides formed by oxidation of ferrous ions in the presence of various bacterial species and inorganic ligands. *Geomicrobiology Journal* 21, 99–112.
- Chenu, C., 1995. Extracellular polysaccharides: an interface between microorganisms and soil constituents. In: Huang, P.M., Berthelin, J., Bollag, J.-M., McGill, W.B., Page, A.L. (Eds.), *Environmental Impact of Soil Component Interactions*. : Natural and Anthropogenic Organics. Lewis, Boca Raton, FL, pp. 217–233.
- Chenu, C., Stotzky, G., 2002. Interactions between microorganisms and soil particles: an overview. In: Huang, P.M., Bollag, J.-M., Senesi, N. (Eds.), *Interactions between Soil Particles and Microorganisms. : Impact on the Terrestrial Ecosystem*. IUPAC Series on Analytical and Physical Chemistry of Environmental Systems. John and Sons, Chichester, pp. 1–40.
- Christensen, A.K., 1971. Frozen thin sections of fresh tissue for electron microscopy, with a description of pancreas and liver. *The Journal of Cell Biology* 51, 772–804.
- Cody, G., Ade, H., Alexander, C., Araki, T., Butterworth, A., Fleckenstein, H., Flynn, G., Gilles, M., Jacobsen, C., Kilcoyne, A., Messenger, K., Sandford, S., Tyliszczak, T., Westphal, A., Wirick, S., Tabuta, H., 2008. Quantitative organic and light-element analysis of comet 81P/Wild 2 particles using C-, N-, and O- μ -XANES. *Meteoritics & Planetary Science* 43, 353–365.
- Crocombe, J.P., Pollak, M., Jollet, F., Thromat, N., Gautier-Soyer, M., 1995. X-ray-absorption spectroscopy at the Fe L_{2,3} threshold in iron oxides. *Physical Review B* 52, 3143–3150.
- Dong, H., 2010. Mineral-microbe interactions: a review. *Frontiers of Earth Science in China* 4, 127–147.
- Doyle, C.S., Traina, S.J., Ruppert, H., Kendelewicz, T., Rehr, J.J., Brown, G.E., 1999. XANES studies at the Al K-edge of aluminum-rich surface phases in the soil environment. *Journal of Synchrotron Radiat* 6, 621–623.
- Dynes, J.J., Tyliszczak, T., Araki, T., Lawrence, J.R., Swerhone, G.D.W., Leppard, G.G., Hitchcock, A.P., 2006. Speciation and quantitative mapping of metal species in microbial biofilms using scanning transmission X-ray microscopy. *Environmental Science and Technology* 40, 1556–1565.
- Ehrlich, H.L., 2002. Interactions between microorganisms and minerals under anaerobic conditions. In: Huang, P.M., Bollag, J.-M., Senesi, N. (Eds.), *Interactions between Soil Particles and Microorganisms. : Impact on the Terrestrial Ecosystem*. IUPAC Series on Analytical and Physical Chemistry of Environmental Systems. John and Sons, Chichester, pp. 459–494.
- FAO-UNESCO, 1997. *Soil Map of the World*, Revised Legend. ISRIC, Wageningen.
- Fleet, M.E., Liu, X., 2009. Calcium L_{2,3}-edge XANES of carbonates, carbonate apatite, and oldhamite (CaS). *American Mineralogist* 94, 1235–1241.
- Francis, J.T., Hitchcock, A.P., 1992. Inner-shell spectroscopy of parabenoquinone, hydroquinone, and phenol: distinguishing quinoid and benzenoid structures. *Journal of Physical Chemistry* 96, 6598–6610.
- Gadd, G.M., 2010. Metals, minerals and microbes: geomicrobiology and bioremediation. *Microbiology* 156, 609–643.
- Gilbert, B., Frazer, B.H., Naab, F., Fournelle, J., Valley, J.W., De Stasio, G., 2003. X-ray absorption spectroscopy of silicates for in situ, sub-micrometer mineral identification. *American Mineralogist* 88, 763–769.
- Giller, K.E., Witter, E., McGrath, S.P., 1998. Toxicity of heavy metals to microorganisms and microbial processes in agricultural soils: a review. *Soil Biology and Biochemistry* 30, 1389–1414.
- Gillespie, A.W., Walley, F.L., Farrell, R.E., Regier, T.Z., Blyth, R.I.R., 2008. Calibration method at the N K-edge using interstitial nitrogen gas in solid-state nitrogen-containing inorganic compounds. *Journal of Synchrotron Radiat* 15, 532–534.
- Gu, B.H., Schmitt, J., Chen, Z., Liang, L.Y., McCarthy, J.F., 1994. Adsorption and desorption of natural organic matter on iron oxide: mechanisms and models. *Environmental Science and Technology* 28, 38–46.
- Guggenberger, G., Haider, K.M., 2002. Effect of mineral colloids on biogeochemical cycling of C, N, P, and S in soil. In: Huang, P.M., Bollag, J.-M., Senesi, N. (Eds.), *Interactions Between Soil Particles and Microorganisms. : Impact on the Terrestrial Ecosystem*. IUPAC Series on Analytical and Physical Chemistry of Environmental Systems. John and Sons, Chichester, pp. 267–322.
- Hitchcock, A.P., 2008. aXis2000 is written in Interactive Data Language (IDL). <http://unicorn.mcmaster.ca/aXis2000.html>.
- Hitchcock, A.P., Mancini, D.C., 1994. Bibliography of atomic and molecular inner-shell excitation studies. *Journal of Electron Spectroscopy and Related Phenomena* 67, 1–132.
- Hitchcock, A.P., Dynes, J.J., Lawrence, J.R., Obst, M., Swerhone, G.D.W., Korber, D.R., Leppard, G.G., 2009. Soft X-ray spectromicroscopy of nickel sorption in a natural river biofilm. *Geobiology* 7, 432–453.
- Horn, R., Smucker, A., 2005. Structure formation and its consequences for gas and water transport in unsaturated arable and forest soils. *Soil and Tillage Research* 82, 5–14.
- Hu, Y.F., Xu, R.K., Dynes, J.J., Blyth, R.I.R., Yu, G., Kozak, L.M., Haung, P.M., 2008. Coordination nature of aluminum (oxy)hydroxides formed under the influence of tannic acid studied by X-ray absorption spectroscopy. *Geochimica et Cosmochimica Acta* 72, 1959–1969.
- Huang, P.M., 2004. Soil mineral-organic matter-microorganism interactions: fundamentals and impacts. *Advances in Agronomy* 82, 391–472.
- Huang, P.M., Germida, J.J., 2002. Chemical and biological processes in the rhizosphere: metal pollutants. In: Huang, P.M., Bollag, J.-M., Senesi, N. (Eds.), *Interactions Between Soil Particles and Microorganisms. : Impact on the Terrestrial Ecosystem*. IUPAC Series on Analytical and Physical Chemistry of Environmental Systems. John and Sons, Chichester, pp. 381–438.
- Hunter, R.C., Hitchcock, A.P., Dynes, J.J., Obst, M., Beveridge, T.J., 2008. Mapping the speciation of iron minerals in *Pseudomonas aeruginosa* biofilms using scanning transmission X-ray microscopy. *Environmental Science and Technology* 42, 8766–8772.
- Ildefonse, P., Cabaret, D., Saintavit, P., Calas, G., Flank, A.M., Lagarde, P., 1998. Aluminum X-ray absorption near edge structure in model compounds and Earth's surface minerals. *Physics and Chemistry of Minerals* 25, 112–121.
- Jacobsen, C., Wirick, S., Flynn, G., Zimba, C., 2000. Soft X-ray spectroscopy from image sequences with sub-100 nm spatial resolution. *Journal of Microscopy* 197, 173–184.
- Jenkinson, D.S., Ladd, J.N., 1981. Microbial biomass in soil: measurement and turnover. In: Paul, E.A., Ladd, J.N. (Eds.), *Soil Biochemistry*. Marcel Dekker, NY, pp. 415–471.
- Jones, D.L., Eldhuset, T., Witb de, H.A., Swensen, B., 2001. Aluminium effects on organic acid mineralization in a Norway spruce forest soil. *Soil Biology and Biochemistry* 33, 1259–1267.
- Kaiser, K., Guggenberger, G., 2000. The role of DOM sorption to mineral surfaces in the preservation of organic matter in soils. *Organic Geochemistry* 31, 711–725.
- Karunakaran, C., 2009. Soft X-ray spectromicroscopy (SM) beamline 10ID-1. Canadian Light Source, Inc. Activity Report 1, 17–217.
- Kaznatchelev, K., Osanna, A., Jacobsen, C., Plashkevych, O., Vahtras, O., Ågren, H., Carravetta, V., Hitchcock, A.P., 2002. Inner-shell absorption spectroscopy of amino acids. *Journal of Chemical Physics* 106, 3153–3168.
- Kaznatchelev, K.V., Karunakaran, C., Lanke, U.D., Urquhart, S.G., Obst, M., Hitchcock, A.P., 2007. Soft X-ray spectromicroscopy beamline at the CLS: commissioning results. *Nuclear Instruments and Methods in Physics Research Section A* 582, 96–99.
- Kinyangi, J., Solomon, D., Liang, B., Lerotic, M., Wirick, S., Lehmann, J., 2006. Nanoscale biogeocomplexity of the organo-mineral assemblage in soil: application of STXM microscopy and C 1s-NEXAFS spectroscopy. *Soil Science Society of America Journal* 70, 1708–1718.
- Kleber, M., Sollins, P., Sutton, R., 2007. A conceptual model of organo-mineral interactions in soils: self-assembly of organic molecular fragments into zonal structures on mineral surfaces. *Biogeochemistry* 85, 9–24.
- Kögel-Knabner, I., 2000. Analytical approaches for characterizing soil organic matter. *Organic Geochemistry* 31, 609–625.
- Konhauser, K.O., Urrutia, M.M., 1999. Bacterial clay authigenesis: a common biochemical process. *Chemical Geology* 61, 399–413.
- Krull, E.S., Bestland, E.A., Gates, W.P., 2002. Soil organic matter decomposition and turnover in a tropical Ultisol: evidence from $\delta^{13}\text{C}$, $\delta^{15}\text{N}$ and geochemistry. *Radio-carbon* 44, 93–112.
- Lal, R., 2004. Soil carbon sequestration impacts on global climate change and food security. *Science* 304, 1623–1626.
- Lawrence, J.R., Swerhone, G.D.W., Leppard, G.G., Araki, T., Zhang, X., West, M.M., Hitchcock, A.P., 2003. Scanning transmission X-ray, laser scanning, and transmission electron microscopy mapping of the exopolymeric matrix of microbial biofilms. *Applied and Environmental Microbiology* 69, 5543–5554.
- Lehmann, J., Solomon, D., Kinyangi, J., Dathe, L., Wirick, S., Jacobson, C., 2008. Spatial complexity of soil organic matter forms at nanometer scales. *Nature Geoscience* 1, 238–242.

- Leinweber, P., Schulten, H.-R., 1998. Nonhydrolyzable organic nitrogen in soil size separates from long-term agricultural experiments. *Soil Science Society of America Journal* 62, 383–393.
- Leinweber, P., Kruse, J., Walley, F.L., Gillespie, A., Eckhardt, K.U., Blyth, R.I.R., Regier, T., 2007. Nitrogen K-edge XANES – an overview of reference compounds used to identify 'unknown' organic nitrogen in environmental samples. *Journal of Synchrotron Radiat* 14, 500–511.
- Lengeler, J.W., Drews, G., Schlegel, H.G., 1999. *Biology of the Prokaryotes*. Blackwell Science, NY.
- Lerotic, M., Jacobsen, C., Schäfer, T., Vogt, S., 2004. Cluster analysis of soft X-ray spectroscopy data. *Ultramicroscopy* 100, 35–57.
- Li, D., Bancroft, G.M., Kasrai, M., Fleet, M.E., Feng, X.H., Tan, K.H., Yang, B.X., 1993. High-resolution Si K- and L_{2,3}-edge XANES of a-quartz and stishovite. *Solid State Communications* 87, 613–617.
- Li, D., Bancroft, G.M., Fleet, M.E., Feng, X.H., 1995a. Silicon K-edge XANES spectra of silicate minerals. *Physics and Chemistry of Minerals* 22, 115–122.
- Li, D., Bancroft, G.M., Fleet, M.E., Feng, X.H., Pan, Y., 1995b. Al K-edge XANES spectra of aluminosilicate minerals. *American Mineralogist* 80, 432–440.
- Liang, B., Lehmann, J., Solomon, D., Kinyangi, J., Grossman, J., O'Neill, B., Skjemstad, J.O., Thies, J., Luizao, F.J., Petersen, J., Neves, E.G., 2006. Black carbon increases cation exchange capacity in soils. *Soil Science Society of America Journal* 70, 1719–1730.
- Lützow, V.M., Kögel-Knabner, I., Ekschmitt, K., Matzner, E., Guggenberger, G., Marschner, B., Flessa, H., 2006. Stabilization of organic matter in temperate soils: mechanisms and their relevance under different soil conditions – a review. *European Journal of Soil Science* 57, 426–445.
- Majestic, B.J., Schauer, J.J., Shafer, M.M., 2007. Application of synchrotron radiation for measurement of iron red-ox speciation in atmospherically processed aerosols. *Atmospheric Chemistry and Physics* 7, 2475–2487.
- Meithke, M., Marahiel, M., 2007. Siderophore-based iron acquisition and pathogen control. *Microbiology and Molecular Biology Reviews* 71, 413–451.
- Naftel, S.J., Sham, T.K., Yiu, Y.M., Yates, B.W., 2001. Calcium L-edge XANES study of some calcium compounds. *Journal of Synchrotron Radiat* 8, 255–257.
- Neilands, J.B., 1995. Siderophores: structure and function of microbial iron transport compounds. *Journal of Biological Chemistry* 270, 26723–26726.
- Nuevola, M., Milama, S.N., Sandforda, S.A., De Gregorius, B.T., Codyd, G.D., Kilcoyne, A.L.D., 2011. XANES analysis of organic residues produced from the UV irradiation of astrophysical ice analogs. *Advances in Space Research* 48, 1126–1135.
- Oades, J.M., 1984. Soil organic matter and structural stability: mechanisms and implications for management. *Plant and Soil* 76, 319–337.
- Obst, M., Dynes, J.J., Lawrence, J.R., Swerhone, G.D.W., Karunakaran, C., Kaznacheyev, K., Benzerara, K., Tylliszczak, T., Hitchcock, A.P., 2009. Precipitation of amorphous CaCO₃ (aragonite) controlled by cyanobacteria: a multi-technique study of the influence of EPS on the nucleation process. *Geochimica et Cosmochimica Acta* 73, 4180–4198.
- Petersen, L., 1976. *Podzols and Podzolization*. DSR Forlag, Copenhagen.
- Politi, Y., Metzler, R.A., Abrecht, M., Gilbert, B., Wilt, F.H., Sagi, I., Addadi, L., Weiner, S., Gilbert, P.U.P.A., 2008. Transformation mechanism of amorphous calcium carbonate into calcite in the sea urchin larval spicule. *Proceedings of the National Academy of Sciences of the United States of America* 45, 17362–17366.
- Samuel, N.T., Lee, C.Y., Gamble, L.J., Fischer, D.A., Castner, D.G., 2006. NEXAFS characterization of DNA components and molecular orientation of surfacebound DNA oligomers. *J. Elec. Spec. Rel. Pheno.* 152, 134–142.
- Sato, S., Solomon, D., Hyland, C., Ketterings, Q.M., Lehmann, J., 2005. Phosphorus speciation in manure and manure-amended soils using XANES spectroscopy. *Environmental Science and Technology* 39 (19), 7485–7491 (2005).
- Schröder, I., Johnson, E., de Vries, S., 2003. Microbial ferric iron reductases. *FEMS Microbiology Reviews* 27, 427–447.
- Schulten, H.-R., Schnitzer, M., 1998. The chemistry of soil organic nitrogen: a review. *Biology and Fertility of Soils* 26, 1–15.
- Schwertmann, U., Kodama, H., Fischer, W.R., 1986. Mutual interactions between organics and iron oxides. In: Huang, P.M., Schnitzer, M. (Eds.), *Interactions of Soil Minerals with Natural Organics and Microbes: Soil Sci. Soc. Am. Spec. Pub.*, 17, pp. 223–250. Madison, WI.
- Seifert, F., Sharp, T., Poe, B., Wu, Z., 1996. ELNES Si L-, K-edge and K-edge spectroscopy as a tool for distinction of four- vs. six-coordinated silicon in high-pressure phases. *Physics and Chemistry of Minerals* 23, 227–227.
- Shang, C., Tiessen, H., 1998. Organic matter stabilization in two semiarid tropical soils: size, density, and magnetic separations. *Soil Science Society of America Journal* 62, 1247–1257.
- Shaw, S.A., Peak, D., Hendry, M.J., 2009. Investigation of acidic dissolution of mixed clays between pH 1.0 and 3.0 using Si and Al X-ray absorption near edge structure. *Geochimica et Cosmochimica Acta* 73, 4151–4165.
- Skjemstad, J.O., Bushby, H.V.A., Hansen, R.W., 1989. Extractable Fe in the surface horizons of a range of soils from Queensland. *Australian Journal of Soil Research* 28, 259–266.
- Smucker, A.J.M., Park, E.J., Dorner, J., Horn, R., 2007. Soil micropore development and contributions to soluble carbon transport within macroaggregates. *Vadose Zone Journal* 6, 282–290.
- Sollins, P., Homann, P., Caldwell, B.A., 1996. Stabilisation and destabilisation of soil organic matter: mechanisms and controls. *Geoderma* 74, 65–105.
- Solomon, J.L., Madix, R.J., Stohr, J., 1991. Orientation and absolute coverage of benzene, aniline, and phenol on Ag(110) determined by NEXAFS and XPS. *Surface Science* 255, 12–30.
- Solomon, D., Lehmann, J., Zech, W., 2001. Land use effects on amino sugar signatures of chromic Luvisols in the semi-arid part of northern Tanzania. *Biology and Fertility of Soils* 33, 33–40.
- Solomon, D., Lehmann, J., Kinyangi, J., Liang, B., Schäfer, T., 2005. Carbon K-edge NEXAFS and FTIR-ATR spectroscopic investigation of organic carbon speciation in soils. *Soil Science Society of America Journal* 69, 107–119.
- Solomon, D., Lehmann, J., Kinyangi, J., Amelung, W., Lobe, I., Ngoze, S., Riha, S., Pell, A., Verchot, L., Mbugua, D., Skjemstad, J., Schäfer, T., 2007a. Long-term impacts of anthropogenic perturbations on the dynamics and molecular speciation of organic carbon in tropical forest and subtropical grassland ecosystems. *Global Change Biology* 13, 511–530.
- Solomon, D., Lehmann, J., Thies, J., Schäfer, T., Liang, B., Kinyangi, J., Neves, E., Petersen, J., Luizao, F., Skjemstad, J., 2007b. Molecular signature and sources of biochemical recalcitrance of organic C in Amazonian Dark Earths. *Geochimica et Cosmochimica Acta* 71, 2285–2298.
- Solomon, D., Lehmann, J., Kinyangi, J., Liang, B., Hanley, K., Heymann, K., Wirick, S., Jacobsen, C., 2009. Carbon (1s) NEXAFS spectroscopy of biogeochemically relevant organic reference compounds. *Soil Science Society of America Journal* 73, 1817–1830.
- Sparks, D.L., 1995. Sorption phenomena in soils. In: Sparks, D.L. (Ed.), *Environmental Physical Chemistry*. Academic Press, NY, pp. 99–139.
- Stöhr, J., Samant, M.G., Lüning, J., Callegari, A.C., Chaudhari, P., Doyle, J.P., Lacey, J.A., Lien, S.A., Purushothaman, S., Speidel, J.L., 2001. Liquid crystal alignment on carbonaceous surfaces with orientational order. *Science* 292, 2299–2302.
- Stotzky, G., 2002. Clays and humic acids affect persistence and biological activity of insecticidal proteins from *Bacillus thuringiensis* in soil. In: Violante, A., Huang, P.M., Bollag, J.-M., Gianfreda, L. (Eds.), *Soil Mineral–Organic Matter–Microorganism Interactions and Ecosystem Health: Ecological Significance of the Interactions Among Clay Minerals, Organic Matter and Soil Biota*. Elsevier, Amsterdam, pp. 1–16.
- Tanner, A., Bornemann, S., 2000. *Bacillus subtilis* YvrK is an acid induced oxalate decarboxylase. *Journal of Bacteriology* 182, 5271–5273.
- Tarnocai, C., Canadell, J.G., Schuur, E.A.G., Kuhry, P., Mazhitova, G., Zimov, S., 2009. Soil organic carbon pools in the northern circumpolar permafrost region. *Global Biogeochemical Cycles* 23, GB2023.
- Templeton, A., Knowles, E., 2009. Microbial transformations of minerals and metals: recent advances in geomicrobiology derived from synchrotron-based X-ray spectroscopy and X-ray microscopy. *Annual Review of Earth and Planetary Sciences* 37, 367–391.
- Theng, B.K.G., 1979. *Formation and Properties of Clay–Polymer Complexes*. Elsevier, New York.
- Thieme, J., Sedlmair, J., Gleber, S.-C., Prietzl, J., Coates, J., Eusterhues, K., Abbt-Braunf, G., Salome, M., 2010. X-ray spectromicroscopy in soil and environmental sciences. *Journal of Synchrotron Radiat* 17, 149–157.
- Tiessen, H., Stewart, J.W.B., Cole, C.V., 1984. Pathways of phosphorous transformations in soils of differing pedogenesis. *Soil Science Society of America Journal* 48, 853–858.
- Torn, M.S., Trumbore, S.E., Chadwick, O.A., Vitousek, P.M., Hendricks, D.M., 1997. Mineral control of soil organic carbon storage and turnover. *Nature* 389, 170–173.
- Trumbore, S., 2009. Radiocarbon and soil carbon dynamics. *Annual Review of Earth and Planetary Sciences* 37, 47–66.
- Tyler, C., Balsberg-Pahlsson, A.M., Bengtsson, G., Baath, E., Tranvik, L., 1989. Heavy metal ecology of terrestrial plants, microorganisms and invertebrates – a review. *Water, Air, & Soil Pollution* 47, 189–215.
- Urquhart, S.G., Turci, C.C., Tylliszczak, T., Brook, M.A., Hitchcock, A.P., 1997. Core excitation spectroscopy of phenyl- and methyl-substituted silanol, disiloxane, and disilane compounds: evidence for π-delocalization across the Si–C_{phenyl} bond. *Organometallics* 16, 2080–2088.
- Urrutia, M.M., Beveridge, T.J., 1994. Formation of fine-grained metal and silicate precipitates on a bacterial surface (*Bacillus subtilis*). *Chemical Geology* 116, 261–280.
- Vairavamurthy, A., Wang, S., 2002. Organic nitrogen in geomacromolecules: Insights on speciation and transformation with K-edge XANES spectroscopy. *Environmental Science and Technology* 36, 3050–3056.
- van Aken, P.A., Liebscher, B., 2002. Quantification of ferrous/ferric ratios in minerals: new evaluation schemes of Fe L_{2,3} electron energy-loss near-edge spectra. *Physics and Chemistry of Minerals* 29, 188–200.
- van Aken, P.A., Liebscher, B., Styrs, V.J., 1998. Quantitative determination of iron oxidation states in minerals using Fe L_{2,3}-edge electron energy-loss near-edge structure spectroscopy. *Physics and Chemistry of Minerals* 25, 323–327.
- Van derlaan, G., Kirkman, I.W., 1992. The 2p absorption spectra of 3d transition metal compounds in tetrahedral and octahedral symmetry. *Journal of Physics: Condensed Matter* 4, 4189–4204.
- Violante, A., Krishnamurti, G.S.R., Huang, P.M., 2002. Impact of organic substances on the formation and transformation of metal oxides in soil environments. In: Huang, P.M., Bollag, J.-M., Senesi, N. (Eds.), *Interactions between Soil Particles and Microorganisms: Impact on the Ecosystem*, IUPAC Series on Analytical and Physical Chemistry of Environmental Systems. John and Sons, Chichester, pp. 133–188.
- Wada, K., 1995. Role of aluminium and iron in the accumulation of organic matter in soils with variable charge. In: Huang, P.M., et al. (Ed.), *Environmental Impact of Soil Component Interactions*. CRC Lewis, 1. Boca Raton, FL, pp. 47–58.
- Wan, J., Tylliszczak, T., Tokunaga, T.K., 2007. Organic carbon distribution, speciation, and elemental correlations within soil microaggregates: applications of STXM and NEXAFS spectroscopy. *Geochimica et Cosmochimica Acta* 71, 5439–5449.
- Wershaw, R.L., Pinckney, D.J., 1980. Isolation and characterization of clay–humic complexes. In: Baker, R.A. (Ed.), *Contaminants and Sediments*. Ann Arbor Science Publishers, Ann Arbor, MI, pp. 207–219.
- Wirick, S., Flynn, G.J., Keller, L.P., Nakamura-Messenger, K., Peltzer, C., Jacobsen, C., Sandford, S., Zolensky, M., 2009. Organic matter from comet 81P/Wild 2, IDPs, and carbonaceous meteorites: similarities and differences. *Meteoritics & Planetary Science* 44, 1611–1626.

- Xiong, W., Peng, J., Hu, Y., 2009. Chemical analysis for optimal synthesis of ferrihydrite-modified diatomite using soft X-ray absorption near-edge structure spectroscopy. *Physics and Chemistry of Minerals* 36, 557–566.
- Yoon, T.H., Johnson, S.B., Benzerara, K., Doyle, C.S., Tyliszczak, T., Shuh, D.K., Brown, G.E., 2004. In-situ characterization of aluminum coating mineral-microorganism aqueous suspensions using scanning transmission X-ray microscopy. *Langmuir* 20, 10361–10366.
- Zubavichus, Y., Shaporenko, A., Grunze, M., Zharnikov, M., 2005. Innershell absorption spectroscopy of amino acids at all relevant absorption edges. *Journal of Physical Chemistry A* 109, 6998–7000.